HOKKAIDO UNIVERSITY

Title	Studies on Mechanical Properties of In-vivo Tissue Formation and In-situ Adaptation Processes in Regenerative Medicine Based on In-Body Tissue Architecture (iBTA)
Author(s)	寺澤, 武
Citation	北海道大学. 博士(工学) 甲第13688号
Issue Date	2019-03-25
DOI	10.14943/doctoral.k13688
Doc URL	http://hdl.handle.net/2115/74123
Type	theses (doctoral)
File Information	Takeshi_Terazawa.pdf

Instructions for use

Hokkaido University Collection of Scholarly and Academic Papers : HUSCAP

Studies on Mechanical Properties of In-vivo Tissue Formation and In-situ Adaptation Processes in Regenerative Medicine Based on In-Body Tissue Architecture (iBTA)

（生体内組織形成術（iBTA）を基盤とする再生医療における組織構築並びに自己化過程の機械的特性に関する研究）

Graduate School of Chemical Sciences and Engineering

Hokkaido University

Takeshi Terazawa

2018

Table of Contents

Table of Contents …… i

Chapter 1 General Introduction …… 1

1.1 Clinical background …… 1

1.2 Implantatable biomaterials …… 1

1.2.1 Artifical grafts …… 1

1.2.2 Autografts …… 2

1.2.3 Allografts and xenografts …… 3

1.2.4 In vitro tissue-engineered biomaterials …… 4

1.3 Concept of in-body tissue architecture (iBTA) …… 4

1.4 Measurement methods of mechanical properties of living soft tissues …… 5

1.5 Thesis outline …… 6

1.6 References …… 8

Chapter 2 In-vivo formation and mechanical properties of iBTA-induced tissues

2.1 Ethanol treatment effect of iBTA-induced tubular tissues (Biotubes) …… 17

2.1.1 Introduction …… 17

2.1.2 Materials and methods …… 18

2.1.3 Result 21
2.1.4 Discussion 23
2.1.5 Conclusion 25
2.1.6 References 26

2.2 Wall thickness control of iBTA-induced Biotubes 33
2.2.1 Introduction 33
2.2.2 Materials and methods 34
2.2.3 Result 36
2.2.4 Discussion 37
2.2.5 Conclusion 39
2.2.6 References 40

2.3 Possibility to aortic valve reconstruction materials of
iBTA-induced sheet-like tissues (Biosheets) 44
2.3.1 Introduction 44
2.3.2 Materials and methods 45
2.3.3 Result 48
2.3.4 Discussion 51
2.3.5 Conclusion 54
2.3.6 References 56

Chapter 3 In-situ mechanical adaptation of iBTA-induced tissues after animal implantations

3.1 Acute phase evaluation of Biosheets after implantation to beagle diaphragms …… 66
3.1.1 Introduction …… 66
3.1.2 Materials and methods …… 67
3.1.3 Result …… 70
3.1.4 Discussion …… 72
3.1.5 Conclusion …… 74
3.1.6 References …… 76

3.2 Chronic phase evaluation of Biosheets after implantation to beagle abdominal wall …… 84
3.1.1 Introduction …… 84
3.1.2 Materials and methods …… 85
3.1.3 Result …… 89
3.1.4 Discussion …… 90
3.1.5 Conclusion …… 93
3.1.6 References …… 94

Chapter 4 Conclusions …… 103
List of Publications …… 106
Acknowledgements …… 110

Chapter 1

General Introduction

1.1 Clinical background

Congenital heart disease (CHD) is a common birth defect and develops in approximately 8 in 1000 births. Septal defects and heart valve dysfunction of CHD patients are one of the main causes of death 1 year after birth [1-2]. Valvular disease acquired from sequelae of rheumatic fever [3], aortic valve stenosis owing to calcification accompanying aging, and mitral regurgitation caused by tissue weakness owing to valve degeneration, is increasing [4].

Omphaloceles, gastroschisis, and congenital diaphragmic hernia are also congenital defects with a high mortality rate [5]. In adults, an inguinal hernia occurs more frequently in men 40 and older, owing to weakened tissues of the body caused by aging [6]. When the body tissue is a defect owing to a congenital defect, aging, or an accident, and the defect is small, self-healing or direct suturing is performed; however, when the defect is large, a graft material is required [5].

1.2 Implantable biomaterials

1.2.1 Artificial grafts

Autografts, allografts obtained from cadavers, and xenografts obtained from porcine and bovine, are used as graft materials, and artificial materials are widely used

based on their availability. Expanded polytetrafluoroethylene (ePTFE), which is a representative artificial material, is used as an artificial blood vessel in tubular form and, in the mesh sheet form, is used for hernia repair [7-8]. For valvular disease, valve replacement surgery with mechanical valves made of carbon is widely performed [9]. The use of artificial materials as the restorative material allows free design of the shape. The artificial materials are strong and mass production is possible. However, artificial materials are vulnerable to infection [10]. Pediatric adaptation to an abdominal hernia is not suitable owing to wound collapse, which could be caused by a foreign body response [5]. In addition, if infection occurs, there is a risk of reoperation. When artificial materials are used for restoring the cardiovascular system, such as a heart valve and blood vessel, the blood adheres to the artificial material, and a thrombus is formed. Therefore, anti-thrombotic drugs, such as warfarin, are required for the lifetime of the patient, and the quality of life, such as restriction of ingestible foods, is lowered. Anticoagulants, such as warfarin, are generally contraindicated for pregnant women [11-12]. Therefore, tissues derived from living bodies with a high antithrombogenicity are used. For heart valve surgery, a biological valve made of bovine, pig, etc. is used. However, there is a problem in durability, re-operation is necessary for 10 to 15 years, so users are limited [13-14].

1.2.2 Autografts

Autografts are often used as graft materials because they do not cause antigenic reactions, are resistant to infection, do not form thrombi, and are inexpensive. For example, the internal thoracic vein is used in the bypass operation of the coronary artery, and in heart valve repair, the pericardium is used as the graft material [15-16]. In addition, autologous auricular cartilage is transplanted in nasal cosmetic formation [17]. However,

it cannot be used when a sufficient amount cannot be collected or when it has been used in a previous surgery. In addition, the size is inappropriate, and the mechanical strength could be insufficient. When using the pericardium for heart valve repair, the strength is insufficient because the pericardium is thin; therefore, the strength should be improved by a glutaraldehyde treatment [16].

1.2.3 Allografts and xenografts

Allografts or xenografts are resistant to infection and biocompatible, and when used for cardiovascular repair, anticoagulants are not required. However, currently, the durability after transplant can be inadequate, and the reoperation risk is higher than that of a mechanical valve [18-19]. Calcification is one of the causes of deterioration, correlation with immune response to tissues has been recognized, and it is thought to be due to glutaraldehyde treatment to suppress antigenicity [20-21]. Recently, a decellularization treatment for suppressing an immune reaction has been developed [22-23]. Issues, such as calcification, could be mediated by functioning as a scaffold of cells by decellularization [24]; however, the strength could be lowered depending on the method, and further development is required [25].

1.2.4 In vitro tissue-engineered biomaterials

The shape of autologous, allogeneic, and xenogeneic tissues used as graft materials cannot be optimally designed to provide the proper shape and strength for the transplant location. An ideal graft material would be an autologous tissue in a free shape. Therefore, a previous study has evaluated in vitro tissue formation using tissue

engineering technology. Representative examples include the cell sheet engineering method involving laminating cells using a special culture dish and forming a tubular shape [26] and the use of a bio 3D printer, which stacks self cells using a stereoscopic method. These methods could be used to create a shape design for blood vessel and hernia applications [27-28]. However, currently, it is difficult to artificially construct a vascular network that nourishes cells forming tissues and to form thick tissue [29]. For example, the strength of the restorative material is assumed insufficient for a part requiring strength, such as the abdominal wall and diaphragmatic hernia in humans and large animals. To adapt the mechanical characteristics of a graft material, a technology that can freely design a thick and durable structure is required. However, ideal materials that can be used for implantation have not been developed.

1.3 Concept of in body tissue architecture (iBTA)

In body tissue architecture (iBTA) technology can be used to create ideal materials [30-32]. The iBTA technology implants an arbitrarily designed mold with an internal space in vivo and applies the internally formed tissue as a graft material (Figure 1a). When the mold is implanted subcutaneously, subcutaneous cells enter the inside of the mold, and the tissue is formed by biosynthesizing the protein by newly forming the capillary (Figure 1b). After two months, the tissue is fully formed inside the mold. The formed tissue, referred to as Biotube or Biosheet, has a high biocompatibility and growth potential after implantation (Table 1-1) [33]. If it can be freely designed in size and can be changed in mechanical properties by this technology, it is considered superior to other graft materials (Table 1-1).

In this study, we investigated the controllability of the tissue shape using iBTA

technology and the relationship between the design parameters of the mold and the mechanical properties of the formed tissue. Then, for an aortic valve leaflet application, the required strength was clarified, and the sheet thickness was defined to maintain the hemodynamics. Furthermore, we investigated the temporal change of the mechanical properties of the tissue after implantation to determine its applicability as a graft material.

1.4 Measurement methods for the mechanical properties of living soft tissues

The mechanical properties of biological soft tissues, such as the pericardium and amniotic membrane, have been studied to evaluate their quality and dynamic characteristics as graft materials [34] [35]. The tissues are not uniform in shape (thickness) and are incompressible heterogeneous materials that deform with load. Their properties are nonlinear and anisotropic [36]. Therefore, there is no standard method for evaluation, and whether nominal stress or true stress should be used for the stress expressing material properties is unknown [37].

In this thesis, bulk mechanical properties (shape) and material mechanical properties were considered. The bulk mechanical properties were used as the evaluation indexes of the reliability performance and flexibility of actual implants, and the material mechanical properties were used as the evaluation indexes of the material changes (tissue regeneration). To accurately evaluate soft tissue, an accurate measurement of the shapes of various thicknesses is required without contact and with a high resolution. Optical coherence tomography is a method that provides a tomographic image of tissue using a near-infrared laser. This method is harmless to the human body and is generally used for retinal diagnosis in ophthalmology. The high decomposability and no-contact property of

this method could be applied to shape measurement, and an algorithm was developed and used in this study. The material properties should be analyzed using the true stress-true strain curve because the living soft tissue is incompressible and deforms. This was adopted for the analysis method shown in Figure 1-3.

1.5 Thesis outline

This thesis consists of four chapters. The background related to this research is introduced in Chapter 1.

In Chapter 2, the investigation of the mechanical properties of the in-vivo iBTA-induced tissues are discussed.

In Section 1, the treatment methods on the strength of the iBTA-induced tubular tissues (Biotubes) are mentioned. When the tensile load corresponding to the blood pressure was repeatedly applied, the temporal deformation amount and the change of the mechanical properties before and after the fatigue test were examined for the Biotubes treated at a 10% and 70% concentration.

In Section 2, the relationship between the thickness of the iBTA-induced tissues and their strength are described. The ability to adjust the Biotube wall thickness was examined by changing the distance parameter of the internal gap of the mold. The relationship between the wall thickness and mechanical strength were investigated.

As discussed in Section 3, thin-membrane iBTA-induced tissues (Biosheets) were prepared in goats, and their strength was investigated for an aortic valve reconstruction application. The required mechanical strength was examined from the strength measurement of the human pericardium.

In Chapter 3, the mechanical property changes of the iBTA-induced tissues

(Biosheets) after animal implantation are discussed.

As mentioned in Section 1, the Biosheets were implanted into the diaphragm, and a follow-up observation was conducted in the acute phase.

As discussed in Section 2, the Biosheets were implanted into the abdominal wall, and a follow-up observation was conducted in the chronic phase.

Finally, in Chapter 4, the research summary and conclusions are discussed.

1.6 References

[1] Bernier PL, Stefanescu A, Samoukovic G, Tchervenkov CI. The challenge of congenital heart disease worldwide: epidemiologic and demographic facts. Semin Thorac Cardiovasc Surg Pediatr Card Surg Annu. 2010; 13: 26–34

[2] Webb GD, Smallhorn JF, Therrien J et al. Congenital heart disease P. Libby, R. Bonow, D. Mann (Eds.), Braunwald's heart disease: a textbook of cardiovascular disease 2007, 8th edition, Saunders, Philadelphia, PA

[3] Carapetis JR. The stark reality of rheumatic heart disease. Eur Heart J. 2015; 36: 1070–1073

[4] Nkomo VT, Gardin JM, Skelton TN, Gottdiener JS, Scott CG, Enriquez-Sarano M. Burden of valvular heart diseases: a population-based study. Lancet. 2006; 368: 1005–1011.

[5] Novotny DA, Klein RL, Boeckman CR. Gastroschisis: an 18-year review. J Pediatr Surg. 1993 May; 28(5): 650–2.

[6] Burcharth J, Pedersen M, Bisgaard T, Pedersen C, Rosenberg J. Nationwide prevalence of groin hernia repair. PLoS One. 2013; 8: e54367

[7] Kirkton RD, Prichard HL, Santiago-Maysonet M, Niklason LE, Lawson JH, Dahl SLM. Susceptibility of ePTFE vascular grafts and bioengineered human acellular vessels to infection. J Surg Res. 2018; 221: 143–151.

[8] Stirler VMA, de Haas RJ, Raymakers JTFJ, Rakic S. Persistent posterior seroma after laparoscopic repair of ventral abdominal wall hernias with expanded polytetrafluoroethylene mesh: prevalence, independent predictors and detached tacks: Retrospective review. Hernia. 2018 Apr; 22(2): 285–291.

[9] Mokhles MM, Kortke H, Stierle U, Wagner O, Charitos EI, Bogers AJ, Gummert J, Sievers HH, Takkenberg JJ. Survival comparison of the Ross procedure and mechanical valve replacement with optimal self-management anticoagulation therapy: propensity-matched cohort study. Circulation 2011; 123: 31–38.

[10] Supriya N, Saima A, Peter H. Lin, Carlos F. Bechara, Mohammad D. Mansouri, Rabih O. Darouiche. Bacterial translocation across ePTFE vascular graft surfaces J Infect. 2010 Jun; 60(6): 486–490.

[11] Aydin E, Yapici F. A retrospective analysis of factors influencing re-operation in patients undergoing mechanical valve replacement. Cardiovasc J Afr. 2013; 24: 251–254.

[12] Steinberg ZL, Dominguez-Islas CP, Otto CM, Stout KK, Krieger EV. Maternal and Fetal Outcomes of Anticoagulation in Pregnant Women With Mechanical Heart Valves. J Am Coll Cardiol. 2017; 69: 2681–2691.

[13] El SF, Hassan W, Latroche B, Helaly S, Hegazy H, Shahid M, Mohamed G, Al-Halees Z. Pregnancy has no effect on the rate of structural deterioration of bioprosthetic valves: long-term 18-year follow up results. J Heart Valve Dis. 2005; 14: 481–485.

[14] Minakata K, Tanaka S, Takahara Y, Kaneko T, Usui A, Shimamoto M, Okawa Y, Yaku H, Yamanaka K, Tamura N, Sakata R. Long-term durability of pericardial valves in the aortic position in younger patients: when does reoperation become necessary? J Card Surg. 2015; 30: 405–413.

[15] Janiec M, Nazari Shafti TZ, Dimberg A, Lagerqvist B, Lindblom RPF. Graft failure and recurrence of symptoms after coronary artery bypass grafting. Scand Cardiovasc J. 2018; 52: 113–119.

[16] Ozaki S, Kawase I, Yamashita H, Uchida S, Takatoh M, Kiyohara N. Midterm outcomes after aortic valve neocuspidization with glutaraldehyde-treated autologous pericardium. J Thorac Cardiovasc Surg. 2018; 155: 2379–2387.

[17] Murrell GL. Auricular cartilage grafts and nasal surgery. Laryngoscope. 2004; 114: 2092–2102.

[18] Arabkhani B, Bekkers JA, Andrinopoulou ER, Roos-Hesselink JW, Takkenberg JJ, Bogers AJ. Allografts in aortic position: Insights from a 27-year, single-center prospective study. J Thorac Cardiovasc Surg. 2016; 152: 1572–1579.

[19] Chang Q, Cheng CC, Jing H, Sheng CJ, Wang TY. Cryoprotective Effect and Optimal Concentration of Trehalose on Aortic Valve Homografts. J Heart Valve Dis. 2015; 24: 74–82.

[20] Lou Y, Jing H, Wang T, Wu H. Experimental Study on the In-Vivo Heterotopic Transplantation of Aortic Valved Homografts after De-Endothelialization. J Heart Valve Dis. 2016 Jan; 25(1): 96–103.

[21] Schoen FJ, Levy RJ. Calcification of tissue heart valve substitutes: progress toward understanding and prevention. Ann Thorac Surg 2005; 79: 1072–1080.

[22] Dettin M, Zamuner A, Naso F, Monteleone A, Spina M, Gerosa G. Natural Scaffolds for Regenerative Medicine: Direct Determination of Detergents Entrapped in Decellularized Heart Valves. Biomed Res Int. 2017; 2017: 9274135

[23] Ghetti M, Papa V, Deluca G, Purpura V, Ruscelli P, Melandri D, Capirossi D, Nigrisoli E, Minghetti P, Bondioli E, Cenacchi G. Histological and ultrastructural evaluation of human decellularized matrix as a hernia repair device. Ultrastruct Pathol. 2018; 42: 32–38.

[24] Neumann A, Cebotari S, Tudorache I, Haverich A, Sarikouch S. Heart valve engineering: decellularized allograft matrices in clinical practice. Biomed Tech (Berl). 2013; 58: 453–456.

[25] Liao J, Joyce EM, Sacks MS. Effects of decellularization on the mechanical and structural properties of the porcine aortic valve leaflet. Biomaterials. 2008; 29: 1065–1074.

[26] L'Heureux N, Dusserre N, Konig G, Victor B, Keire P, Wight TN, Chronos NA, Kyles AE, Gregory CR, Hoyt G, Robbins RC, McAllister TN. Human tissue-engineered blood vessels for adult arterial revascularization. Nat Med. 2006; 12: 361–365.

[27] Itoh M, Nakayama K, Noguchi R, Kamohara K, Furukawa K, Uchihashi K, Toda S, Oyama J, Node K, Morita S. Scaffold-Free Tubular Tissues Created by a Bio-3D Printer Undergo Remodeling and Endothelialization when Implanted in Rat Aortae. PLoS One. 2015; 10: e0136681

[28] Zhang XY, Yanagi Y, Sheng Z, Nagata K, Nakayama K, Taguchi T. Regeneration of diaphragm with bio-3D cellular patch. Biomaterials. 2018; 167: 1–14.

[29] Novosel EC, Kleinhans C, Kluger PJ. Vascularization is the key challenge in tissue engineering. Adv Drug Deliv Rev. 2011; 63: 300–311.

[30] Nakayama Y, Kaneko Y, Takewa Y, Okumura N. Mechanical properties of human autologous tubular connective tissues (human biotubes) obtained from patients undergoing peritoneal dialysis. J Biomed Mater Res B Appl Biomater. 2016; 104: 1431–1437.

[31] Yamanami M, Yahata Y, Uechi M, Fujiwara M, Ishibashi-Ueda H, Kanda K, Watanabe T, Tajikawa T, Ohba K, Yaku H, Nakayama Y. Development of a

completely autologous valved conduit with the sinus of Valsalva using in-body tissue architecture technology: a pilot study in pulmonary valve replacement in a beagle model. Circulation. 2010; 122: 100–106

[32] Furukoshi M, Moriwaki T, Nakayama Y. Development of an in vivo tissue-engineered vascular graft with designed wall thickness (biotube type C) based on a novel caged mold. J Artif Organs. 2016; 19: 54–61.

[33] Nakayama Y, Furukoshi M, Feasibility of in-body tissue architecture in pediatric cardiovascular surgery: development of regenerative autologous tissues with growth potential. J. Pediatr. Cardiol. Cardiovasc. Surg. 2018; 2: 28–36

[34] W.P. De Wilde, C.A. Brebbia, U. Mander. High performance structures and materials V. WIT Press; 2010

[35] Yamashita H, Ozaki S, Iwasaki K, Kawase I, Nozawa Y, Umezu M. Tensile Strength of Human Pericardium Treated with Glutaraldehyde. Ann Thorac Cardiovasc Surg 2012; 18: 434–437.

[36] Duprey A, Khanafer K, Schlicht M, Avril S, Williams D, Berguer R. In vitro characterisation of physiological and maximum elastic modulus of ascending thoracic aortic aneurysms using uniaxial tensile testing. Eur J Vasc Endovasc Surg 2010; 39: 700–707.

[37] Gerhard AH, Ray WO. Biomechanics of Soft Tissue in Cardiovascular Systems. Springer-Verlag Wien GmbH; 2003

[38] Campbell GR, Campbell JH. Development of tissue engineered vascular grafts. Curr Pharm Biotechnol. 2007; 8: 43–50.

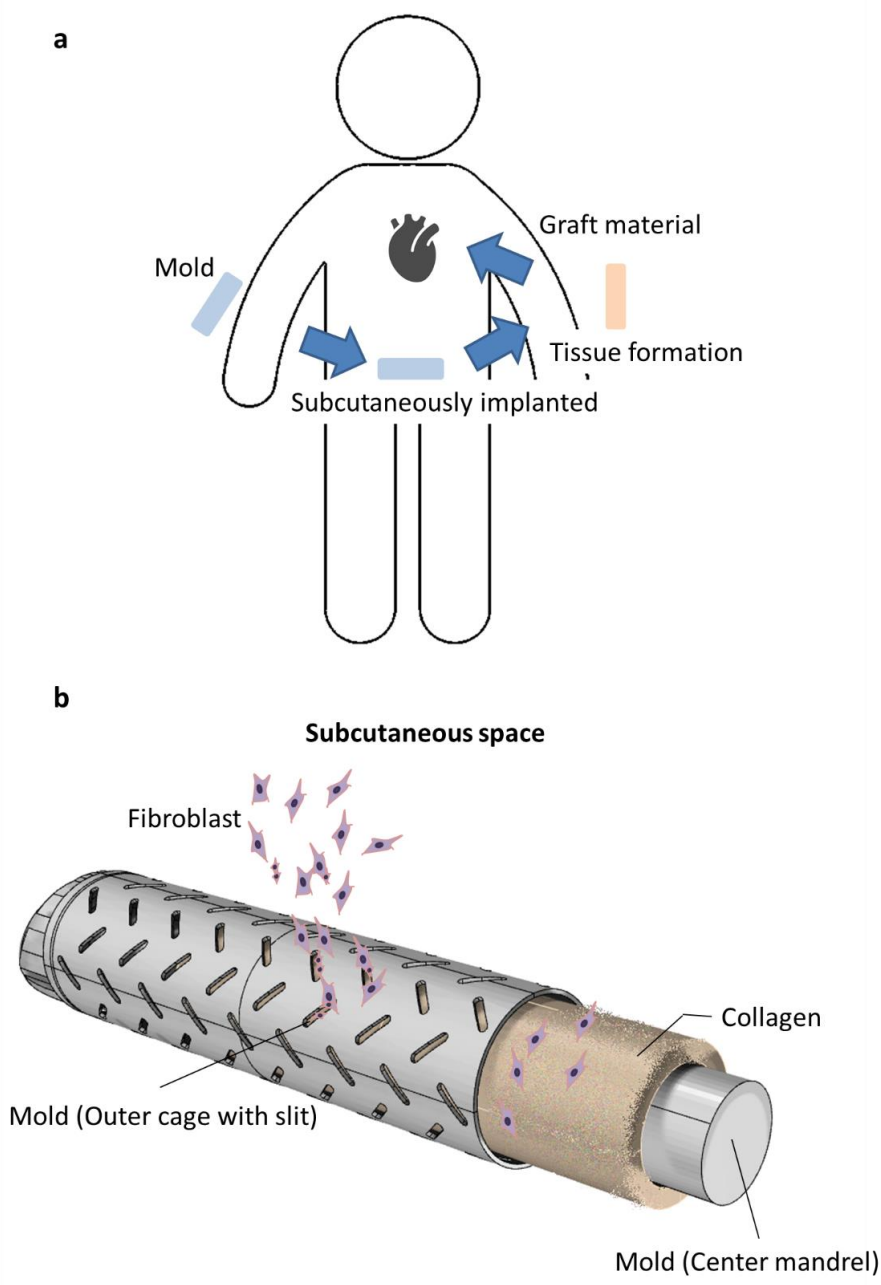

Figure 1-1. (a) Conceptual diagram of the in-body tissue architecture. The tissue formed inside the mold is used as the graft material. Image (b) shows the tissue formation principle of the in-body tissue architecture technology. The mold consists of a center mandrel and outer cage with a slit and cap. The fibroblasts surrounding the mold embedded in the subcutaneous space enter between the center mandrel and outer cage from the slit and form collagen to fill the internal space of the mold.

Table 1-1. Summary of the advantages and disadvantages of the graft materials. This thesis focuses on the shape design performance of the in-body tissue architecture and the suitability of the mechanical properties as a graft material [35].

Biomaterial	Biocompatibility	Thromboresistant Infection resistant	Compliant, elastic	Shape designability	Availability (Ease of manufacture)
Artificial material (polymer etc.)	×	×	△	○	○
Autologous tissue	○	○	○	×	× (Can be used only once)
Allograft	○	○	○	×	△ (To a limited number)
Xenograft	○	○	○	×	○
Cell sheet engineering / Bio3D printing	○	○	○	△ (Limitted to thin tissue)	○
in-Body tissue architecture	○	○	**Focused on this thesis**		○

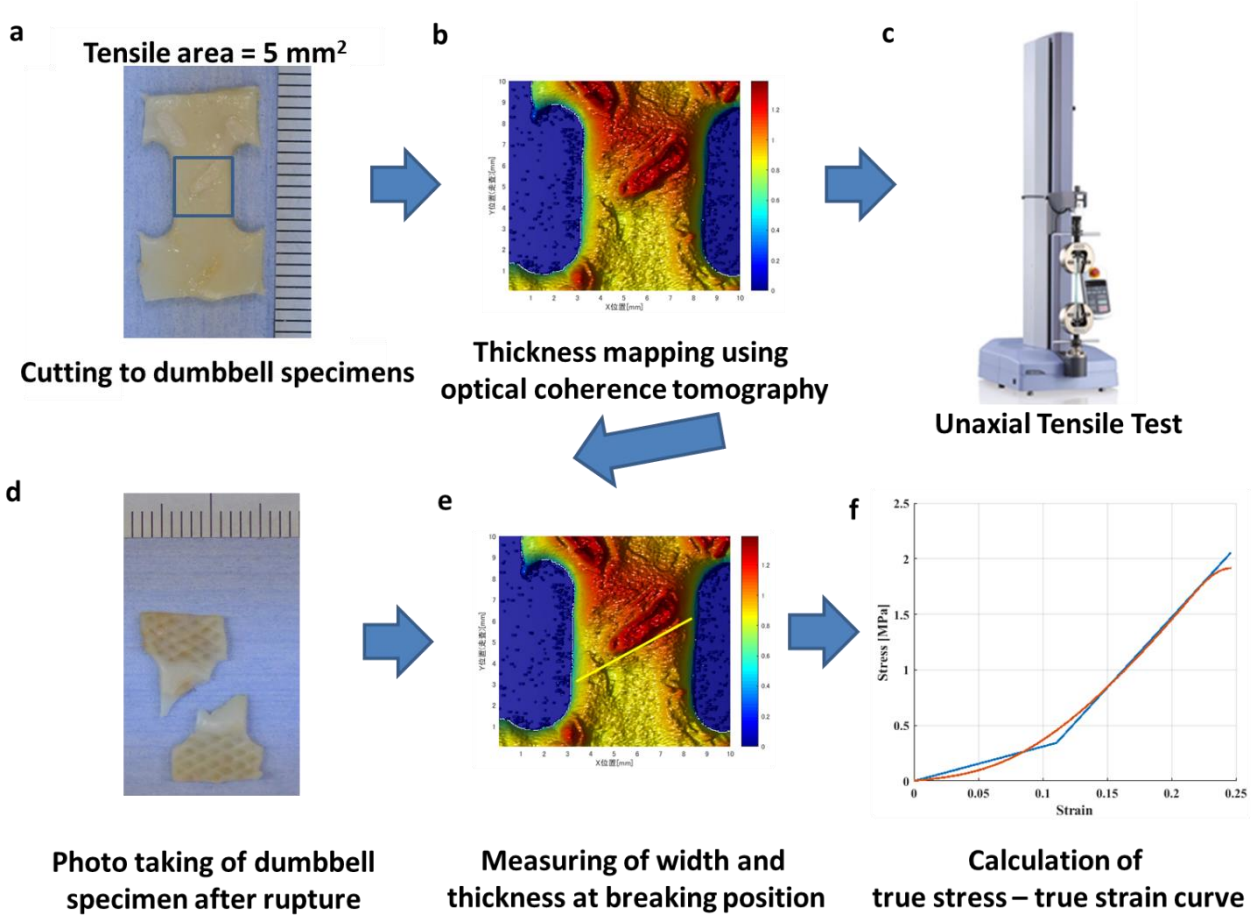

Figure 1-3. Evaluation process of the mechanical properties. An original algorithm for specimen thickness mapping using optical coherence tomography was developed. The thickness of the rupture position and the width of the sample was measured with a high accuracy and without contact in a soft tissue with various thicknesses.

Chapter 2

In-vivo formation and mechanical properties of iBTA-induced tissues

Chapter 2.1

Ethanol treatment effect of iBTA-induced tubular tissues (Biotubes)

2.1.1 Introduction

As tissue-engineered blood vessels (TEBV), cultured blood vessels, such as cytograft [1] and decellularized blood vessels [2], have been developed according to in vitro cell management protocol. Recently, cultured vessels using three-dimensional bio-printers [3] have also been developed. Furthermore, Biotube collagenous tubular tissues have been produced in vivo [4,5]. The mechanical strength of these tissue-engineered vessels is maintained by the extracellular matrixes (ECMs) mainly consisting of collagen. It is desirable to store these tissues easily, without the tissue being deteriorated for a long period until implantation. Methods to store these tissues include cryopreservation, wet preservation, and freeze-drying. Conventional cryopreservation methods damage the ECMs and reduce their mechanical strength [6,7], and therefore, a special equipment has been developed; however, highly reliable sterilization method has not been established [8].

As ethanol can help maintain ECMs cost-effectively at room temperature, it is used to store amniotic membranes [9] or Biotubes [4,5]. Ethanol prevents hydrolysis by water, growth of residual microorganisms, and prevents collagen degradation by

residual endogenous enzymes [10]. On the contrary, as ethanol dehydrates tissues, the degree of contraction and deformation of tissue varies depending on the concentration of ethanol, leading to changes in their strength or compliance.

In this study, the mechanical properties of Biotubes stored in two different concentrations (10% or 70%) of ethanol at room temperature were compared by fatigue and tensile tests.

2.1.2 Materials and methods

2.1.2.1 Ethical approval

All animals received care according to the Principles of Laboratory Animal Care (National Institutes of Health, No. 56-23, received 1985) and the research protocols were approved by the Ethics Committee of National Cerebral and Cardiovascular Center (No. 17013).

2.1.2.2 Preparation of Biotube

According to our previous report [5], Biotubes were prepared by embedding molds (four per goat) in the abdominal subcutaneous pouches of a goat (approximately 40 kg). Briefly, anesthesia was induced with intramuscular (IM) xylazine 2 mg/kg after intra-tracheal intubation, and was maintained by isoflurane inhalation. Two months after the embedding procedure, the molds were harvested and Biotubes (internal diameter 6 mm, wall thickness ca. 2 mm) were extracted by removing the molds. The Biotubes were stored in 10% or 70% ethanol solution for 20 d at room temperature prior to the measurement of mechanical properties.

2.1.2.3 Measurement of wall thickness

Biotubes and goat carotid arteries (CA, internal diameter ca. 5 mm) were cut into 5-mm width pieces (n = 5 in 10%, n = 6 in 70%, n = 5 in CA), and then opened to obtain rectangular samples. The wall thickness mapping of all samples on the whole surface was constructed by optical coherence tomography system (OCT, IVS-2000; Santec, Aichi, Japan). Briefly, the spatial resolution of the OCT was 0.0391 mm in surface length and 0.008 mm in depth. The sample was placed with its smooth surface in contact with the stage and laser light was irradiated perpendicularly to the stage surface. An algorithm was developed to calculate the thickness distribution by determining the local maximum point of reflection intensity closest to the depth direction from the irradiation position as the sample surface position. Subsequently, the thickness data along the longitudinal axis close to the breaking position was obtained; the average value of sampling data was defined as the thickness at the breaking point.

2.1.2.4 Fatigue test

The samples were fixed with clamps (distance: 5 mm) and repeatedly loaded by a tensile system (MMT-250NV-10; Shimadzu, Japan). For each sample, a tension of 0.2–0.32 N, corresponding to the aortic pressure of 80–120 mmHg, was applied by upper chuck moved at a frequency of 10 Hz and was repeated 700,000 times (7 d in terms of heartbeat of 70 bpm). The sample was then bathed with saline circulated by a pump and maintained wet. The elongation of sample was measured by the distance between the chucks, and the load applied to the sample was also measured. After the cyclic load test, the thickness of tissue was measured by OCT.

2.1.2.5 Measurement of breaking strength

Tissue strength was measured using cyclic loaded samples and unloaded control sample with a uniaxial tensile tester (EZ-LX; Shimadzu, Kyoto, Japan). The sample was fixed at a distance of 5 mm with two chucks in order to extend it in the circumferential direction. The distance between the chucks was preloaded with a load of 0.02 N and thereafter the initial length of the sample obtained. The load was applied at a speed of 0.5 mm/s until it fractured. The breaking strength was defined as the maximum load value (N) at the highest point of the obtained load-extension curve. The unit-breaking strength was defined as a value obtained by dividing the breaking strength by the sample width.

2.1.2.6 Calculation of mechanical values

True stress/true strain was calculated according to a previously published method [11], using the thickness of the breaking position measured with the OCT, and the load and displacement was measured with a tensile tester. The ultimate tensile strength (MPa) was determined from the maximum value of stress and Young's modulus (MPa) was determined from the maximum slope of the stress-strain curve.

The physiological modulus was calculated according to a previously published method [11]. From the Laplace equation, the relationship between the stress in the circumferential direction as following formula:

$$D_i = D_0 (1 + \varepsilon)$$

$$\sigma = (P_i \times D_i) / (2 \times t)$$

Where, σ is the circumferential stress of tube, P_i is the blood pressure, D_0 is the initial internal diameter, D_i is the internal diameter, ε is the strain of each sample, and t

is wall thickness. Physiological modulus is a gradient value calculated from slope from circumferential stress and strain of 80 mmHg and 120 mmHg.

The burst strength was calculated using the following formula:

$$P = 2F / L_0 D_i$$

where, P is the estimated burst pressure, F is the breaking strength, and L_0 is the initial sample length of the ring sample.

2.1.2.7 Statistical analyses

The results are expressed as mean ± standard deviation. The differences in mean values between groups were examined by the t test and the differences with a p value of < 0.05 were considered significant.

2.1.3 Results

Biotubes were obtained as a tubular tissue in spiral shape with an internal diameter and length of approximately 6 mm and 25 cm, respectively (Figure 2-1-1a). A part of Biotube was randomly cut to a width of 5 mm, and then a rectangular sample [5 mm × 18 mm) was obtained by cutting in longitudinal direction (Figure 2-1-1b). A typical example of the wall thickness mapping of the original samples after storing in each ethanol solution constructed by OCT system is shown in Figure 2-1-1c, d. When stored in 10% solution, the averaged thickness of the sample was 1.84 ± 0.14 mm, but was 1.52 ± 0.29 mm after storing in 70% solution (Figure 2-1-1e, f).

After the fatigue test, the thickness of the 10%-sample decreased significantly to 1.14 ± 0.22 mm, but there was no significant change in the 70%-sample (Figure 2-1-1e, f). The length of the samples continuously elongated during the fatigue test in both

ethanol solutions (Figure 2-1-2). The difference in the elongation between two samples was gradually spreaded, with a significant difference at p value < 0.05 after 350,000 cycles, p < 0.01 after 450,000 cycles. After 700,000 cycles, the elongation ratio of the 10%-sample was 76.8 ± 24.2%, and that of the 70%-sample was 17.8 ± 11.5%.

The typical stress-strain curves of samples before and after the fatigue test were shown in Figure 2-1-3. Almost similar curves were obtained in 70%-sample, but in 10%-sample marked deviation in the stress was observed. The mechanical properties obtained from the stress-strain curves are summarized in Figure 2-1-4. The ultimate tensile strength after the fatigue test was significantly higher in the 10%-sample, but the unit length-breaking load representing the actual strength was equivalent before and after the fatigue test. In the 70%-sample, no significant difference was observed between tensile strength and breaking strength before and after the fatigue test. The ultimate tensile strength of goat carotid artery was at least 8 times higher than any conditions of the Biotubes. The difference in Young's modulus was also found to be significant before and after the fatigue test in the 10%-sample. The physiological modulus of the 70%-sample was higher than that of the 10%-sample. The physiological modulus, which is rigid in the strain range at arterial pressure, was higher in the 70%-sample than in the 10%-sample. In addition, the physiological modulus of 10%-sample also increased significantly before and after the fatigue test. The goat carotid artery was lower in physiological modulus than the Biotube, but Young 's modulus was higher. The fracture strain and estimated burst pressure did not exhibit significant difference before and after the fatigue test. And also, the fracture strain was significantly smaller in the after fatigue test than in the 70%-sample in the 10% sample. In the comparison after the fatigue test, the fracture strain of the 10%-sample was

significantly smaller than the 70%-sample. The goat carotid artery was about 3 times the fracture strain of Biotubes.

2.1.4. Discussion

In the present study, I focused on the concentration of ethanol used for the store of Biotubes and studied the relationship between shape and mechanical properties. Even with the wall tension generated at the blood pressure level, elongation occurred when stored in low concentration (10%) of ethanol, and the wall thickness was thin. Although the tensile strength and Young's modulus of the sample increased before and after stretching, the breaking strength was equivalent. After the fatigue test, physiological modulus increased in the 10%-sample, the fracture strain of the 10%-sample was smaller than the 70%-sample and it was difficult to stretch and fracture strain of the 10%-sample was also decreased. Contrarily, store in 70% ethanol showed no significant changes in ultimate tensile strength, and breaking strength was observed before and after the fatigue test.

The transplantation of amniotic membrane into the cornea has been reported. The interstitial tissue, which is the substantial tissue of the amniotic membrane, is a tissue composed mainly of collagen, and it has been conventionally cryopreserved [12]. However, cryopreservation not only requires large-scale facilities, but also there is a concern that the ECM will be destroyed [13]. A special dry method has also been developed with need of complicated protocols [14,15]. On the other hand, glutaraldehyde solution can improve the tissue strength and elastic modulus by chemical cross-linking [16]. However, it is one of major factors for calcification after implantation [17]. In clinical organ transplantation, human aorta was stored by

refrigeration with Euro-Collins solution known as an organ preservation solution [18]. There was no significant change in its mechanical property even after store at 4 °C for 31 days. However, because there is no sterilization function in the preservation solution, careful clean management is needed.

Differences based on ethanol concentrations appeared in the strain and physiological modulus of the Biotube. The elongation of Biotube preserved in 10% ethanol was higher than that of Biotubes stored in 70% ethanol. With the elongation of the wall of Biotube, the internal diameter of the tube increases. According to Laplace's law, the internal diameter of the tube is proportional to the wall tension, and therefore, expansion of the internal diameter results in an increase in wall tension. Therefore, even if the breaking strength is equal, the burst pressure decreases as the internal diameter increases. There is also the possibility of development of aneurysm when transplanting a Biotube preserved with low concentration ethanol into an artery. As a result, a thrombus might form within the artery with aneurysm, causing cerebral infarction or myocardial infarction [19,20]. Although no significant difference was observed in this study, the degree of decrease in the burst average value was high when the Biotubes were stored in 10% ethanol. Theoretically, it is thought that the influence of elongation increases as the internal diameter of the tube increases. It seems that ethanol can increase practical compliance and prevent elongation. Therefore, untreated Biotubes are deemed inappropriate for transplantation, and from the viewpoint of ease of expansion, it may be better to treat 70% ethanol.

The rate of elongation was significantly different between the samples at 350,000 cycles, which is equivalent to 3.5 d at a heart rate of 70 bpm. Approximately 15% strain occurred even when stored in 70%, it may be better for the concentration to be higher,

so its optimization is a future task. In fact, it is thought that the Biotube made of collagen functions as a cell scaffold in vivo after transplantation and the tube is strengthened by matrix formation of the migrated cells. Further studies are needed to determine how dynamically the changes in physical property occur.

2.1.5 Conclusion

There was no significant decrease in the strength of Biotubes stored in 10% and 70% ethanol solutions at room temperature even with repeated tension generated by aortic pressure. However, after repeated loading, the elongation of Biotubes stored in 10% ethanol was higher than that of Biotubes stored in 70% ethanol; this might induce aortic aneurysm when transplanted into the aorta. Storing Biotubes in high concentration ethanol solution improved practical compliance and prevented stretching. The preservation of ECM with 70% ethanol is a cost effective, saft and easy method.

2.1.6 References

[1] L'Heureux N, Dusserre N, Konig G, Victor B, Keire P, Wight TN, Chronos NA, Kyles AE, Gregory CR, Hoyt G, Robbins RC, McAllister TN. Human tissue-engineered blood vessels for adult arterial revascularization. Nat Med. 2006;12:361-5.

[2] Olausson M, Patil PB, Kuna VK, Chougule P, Hernandez N, Methe K, Kullberg-Lindh C, Borg H, Ejnell H, Sumitran-Holgersson S. Transplantation of an allogeneic vein bioengineered with autologous stem cells: a proof-of-concept study, Lancet 2012;21:230-7.

[3] Itoh M, Nakayama K, Noguchi R, Kamohara K, Furukawa K, Uchihashi K, Toda S, Oyama J, Node K, Morita S. Scaffold-Free Tubular Tissues Created by a Bio-3D Printer Undergo Remodeling and Endothelialization when Implanted in Rat Aortae, PLoS One 2015;10:e0136681.

[4] Nakayama Y, Furukoshi M. Feasibility of in-body tissue architecture in pediatric cardiovascular surgery: development of regenerative autologous tissues with growth potential. J Pediatr Cardiol Cardiac Surg. 2018;2:28-36.

[5] Nakayama Y, Furukoshi M, Terazawa T, Iwai R. Development of long in vivo tissue-engineered "Biotube" vascular grafts. Biomaterials. 2018;185:232-239.

[6] Dahl SL, Chen Z, Solan AK, Brockbank KG, Niklason LE, Song YC. Feasibility of vitrification as a storage method for tissue-engineered blood vessels. Tissue Eng.,2016;12:291-300.

[7] Elder E, Chen Z, Ensley A, Nerem R, Brockbank K, Song Y. Enhanced tissue strength in cryopreserved, collagen-based blood vessel constructs. Transplant Proc. 2005;37:4625-9.

[8] Kitagawa K, Yanagisawa S, Watanabe K, Yunoki T, Hayashi A, Okabe M, Nikaido T. A hyperdry amniotic membrane patch using a tissue adhesive for corneal perforations and bleb leaks. Am J Ophthalmol. 2009;148:383-9.

[9] Lyons GD, Dyer RF, Ruby JR. Morphologic analysis of tympanic membrane grafts. Laryngoscope 1977;87:1705-9.

[10] Mohammad ZA, James HH IV. Skin Tissue Engineering and Regenerative Medicine. 1st ed. Academic Press; 2016.

[11] Duprey A, Khanafer K, Schlicht M, Avril S, Williams D, Berguer R. In vitro characterisation of physiological and maximum elastic modulus of ascending thoracic aortic aneurysms using uniaxial tensile testing. Eur J Vasc Endovasc Surg. 2010;39:700-7.

[12] Laustsen J, Paaske WP, Oyre S, Pedersen EM. Dynamic quantification, visualisation and animation of blood velocities and flows in infrarenal aortic aneurysms in vivo by three-dimensional MR phase velocity encoding. Eur J Vasc Endovasc Surg. 1995;9:383-8.

[13] Dahl SL, Chen Z, Solan AK, Brockbank KG, Niklason LE, Song YC. Feasibility of vitrification as a storage method for tissue-engineered blood vessels, Tissue Eng. 2006;12:291-300.

[14] Thomasen H, Pauklin M, Steuhl KP, Meller D. Comparison of cryopreserved and air-dried human amniotic membrane for ophthalmologic applications, Graefes Arch Clin Exp Ophthalmol, 2009;247:1691-700.

[15] Toda A, Okabe M, Yoshida T, Nikaido T. The potential of amniotic membrane/amnion-derived cells for regeneration of various tissues, J Pharmacol Sci. 2007;105:215-28.

[16] Yamashita H, Ozaki S, Iwasaki K, Kawase I, Nozawa Y, Umezu M. Tensile strength of human pericardium treated with glutaraldehyde. Ann Thorac Cardiovasc Surg, 2012;18:434-7.

[17] Schoen FJ, Levy RJ. Calcification of tissue heart valve substitutes: progress toward understanding and prevention. Ann Thorac Surg. 2005;79:1072-80.

[18] Adham M, Gournier JP, Favre JP, De La Roche E, Ducerf C, Baulieux J, Barral X, Pouyet M. Mechanical characteristics of fresh and frozen human descending thoracic aorta. J Surg Res. 1996;64:32-4.

[19] Calviere L, Viguier A, Da Silva NA Jr, Cognard C, Larrue V. Unruptured intracranial aneurysm as a cause of cerebral ischemia. Clin Neurol Neurosurg, 2011;113:28-33.

[20] Shaikh AH, Hanif B, Hassan K, Nasir S. Coronary aneurysm complicated by acute myocardial infarction. J Pak Med Assoc. 2012;62:854-6.

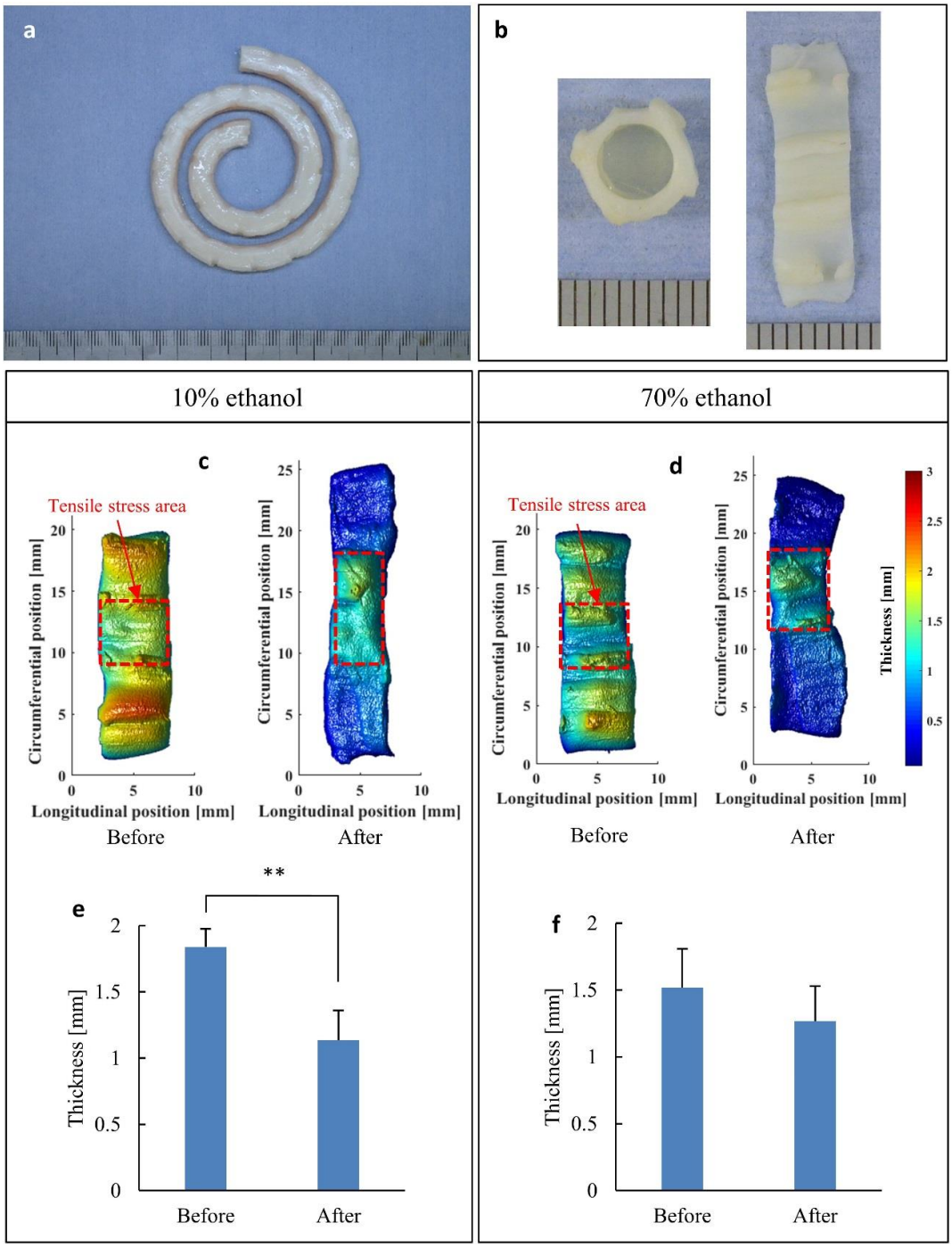

Figure 2-1-1. Images of the Biotube obtained from the mold (a) and cross-sectional view of the Biotube and Biotube rectangular sample stored in 70% ethanol solution (b). Thickness mapping by OCT of the sample stored in 10% (c) or 70% ethanol (d) before and after the fatigue test. The average and standard deviation of the thickness of the tensile stress area of the samples stored in 10% (e) or 70% ethanol (f) before and after the fatigue test. The significance levels by statistical analysis are ** $p < 0.01$.

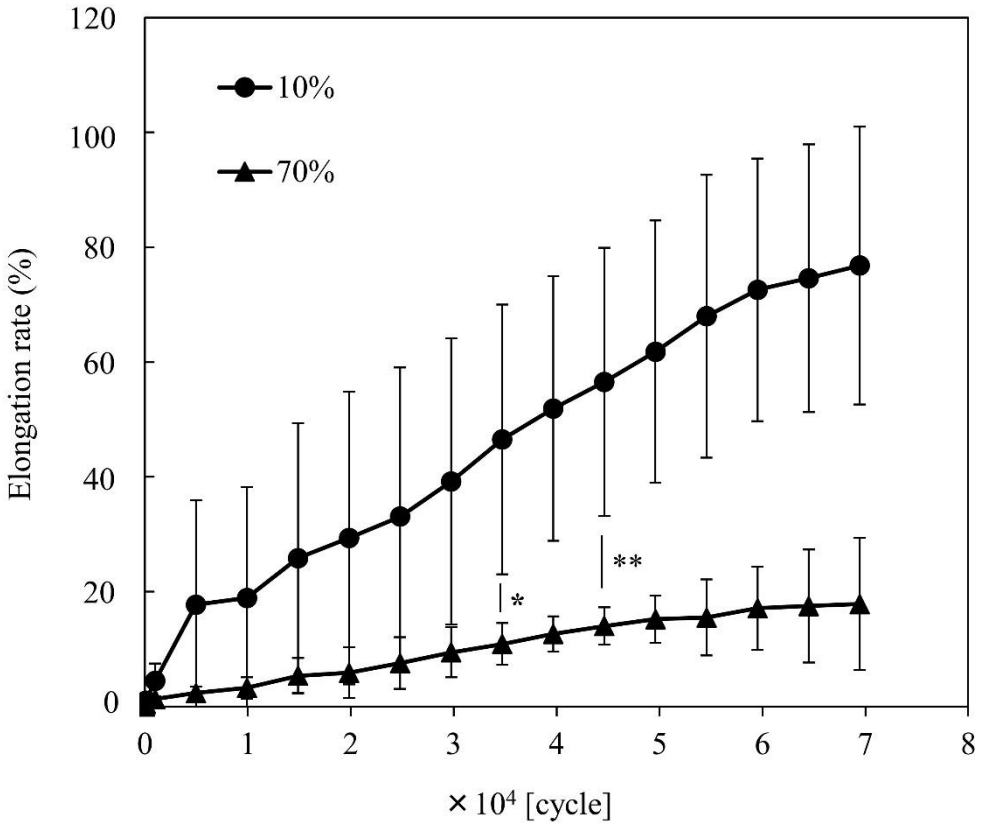

Figure 2-1-2. Relationship between the number of cycles in the fatigue test and strain of the Biotube samples. The significance levels by statistical analysis are * $p < 0.05$ and ** $p < 0.01$.

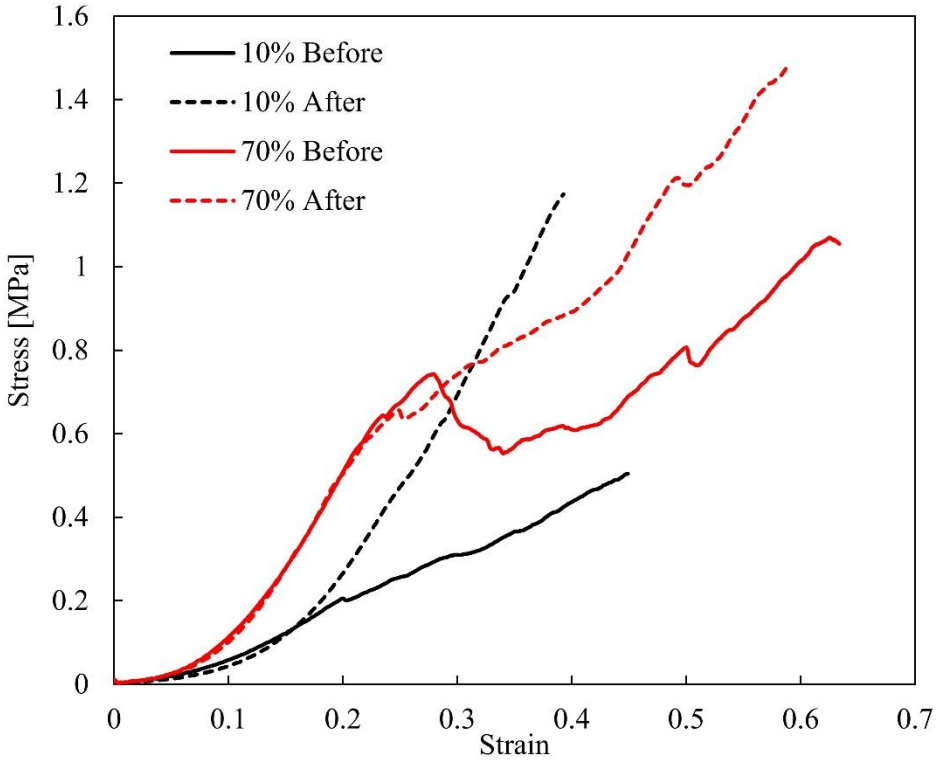

Figure 2-1-3. Stress – strain curve of Biotube samples stored in 10% or 70% ethanol before and after the fatigue test. A goat carotid artery's curve is also plotted. Curves are showed by the average line for each condition

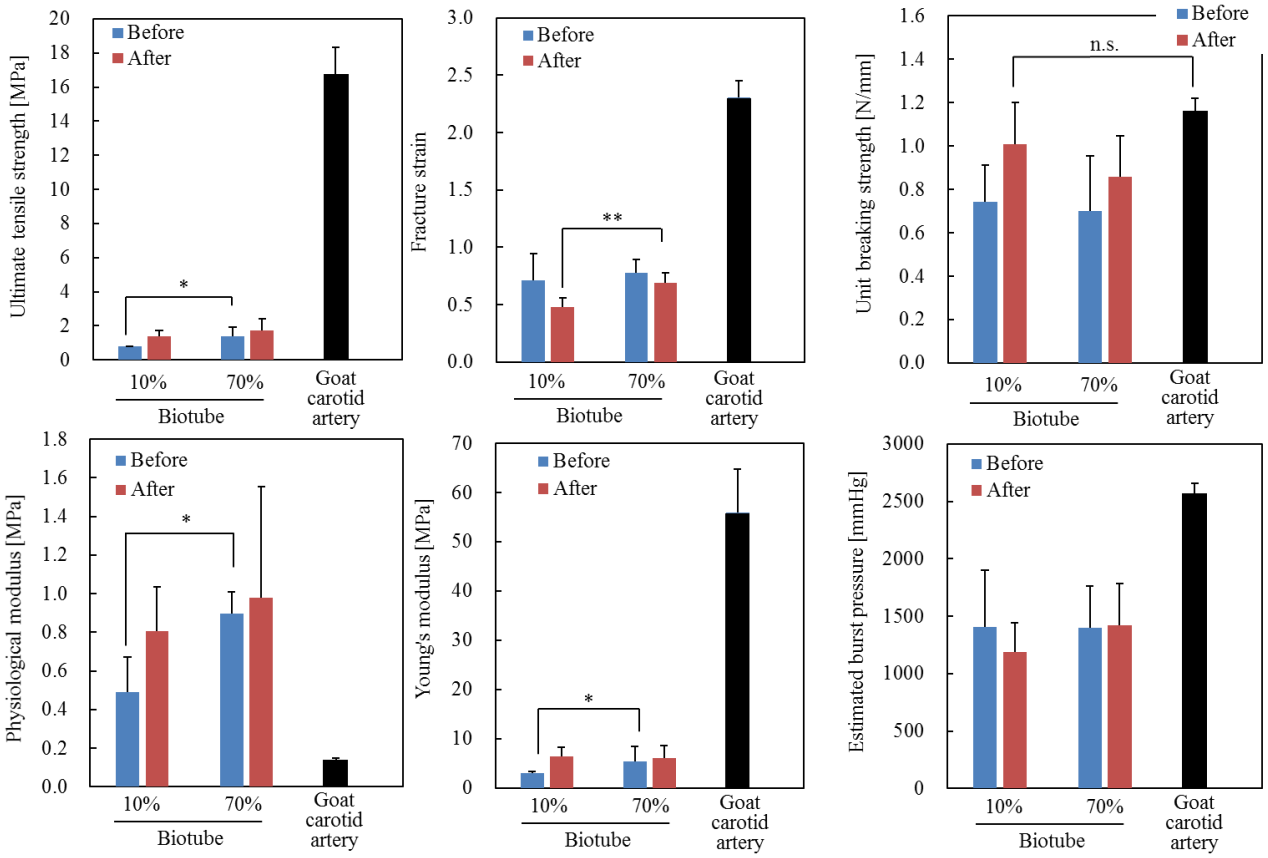

Figure 2-1-4. Physical properties of Biotube samples stored in 10% or 70% ethanol before and after the fatigue test, and goat carotid artery. The significance levels by statistical analysis are * $p < 0.05$ and ** $p < 0.01$. $p < 0.01$ was observed in all goat carotid artery cases, except for the unit breaking strength.

Chapter 2.2

Wall thickness control of iBTA-induced Biotubes

2.2.1 Introduction

In-body tissue architecture (IBTA) is an in vivo tissue-engineering technology used to prepare autologous or allogenic implantable tissues [1]. In classical IBTA, foreign materials are encapsulated primarily by fibroblasts and collagen fibers. However, the walls of the obtained tissues are very thin (<0.1 mm) because these tissues encapsulate only the surface of a simple silicone rod [2]. Recently, thick and strong small-caliber tubular structures with an inner diameter of 2 mm have been formed by developing a new-concept IBTA using a type-C mold, which has a cage with slits surrounding a silicone center rod [2]. Tissues with approximately 1-mm thickness are formed by cell migration through the slits to the rod–cage gap.

In this study, large-sized type-C molds were designed for preparing large Biotubes with the inner diameter ranging from 11 to 17 mm. The wall thickness of these Biotubes could be controlled by changing the rod–cage gap in the molds. Furthermore, the mechanical/histological properties of the Biotubes were evaluated to verify their application to grafts for various tubular or sheet-like tissues such as tracheae, esophagi, or pericardia.

2.2.2 Materials and methods

2.2.2.1 Preparation of molds

Four types of molds were prepared by changing the rod–cage gap. The molds were assembled using three parts: a silicone center rod (outer diameter: 11, 13, 15, or 17 mm), a stainless-steel cage (internal diameter: 19 mm) with several slits (8 × 2 mm), and plastic caps made using a 3D digital printer (ProJet 3510 HD Plus, 3D Systems, Rock Hill, SC) (Figure 2-2-1A).

2.2.2.2 Ethical approval

All animals received care according to the Principles of Laboratory Animal Care (National Institutes of Health, No. 56-23, received 1985), and the research protocols were approved by the ethics committee of National Cerebral and Cardiovascular Center (No. 17013) and Hokkaido University (No. 16-0110). The clinical research process involving human pericardium was approved by the ethics committee of the National Cerebral and Cardiovascular Center (No. M27-054) and of the Oita University (No.868).

2.2.2.3 Preparation of Biotubes

Four types of molds (n = 3 for each type) were surgically embedded in the abdominal subcutaneous pouches of three Holstein cows (body weight: approximately 700 kg) under the combination of epidural and infiltration anesthesia. After 8–12 weeks, the molds were harvested with the surrounding connective tissues. Biotubes were obtained by removing the mold materials along with the surrounding connective tissues and were then stored in a 70% ethanol solution.

2.2.2.4 Preparation of control samples

Three types of arteries (ascending aorta (inner diameter: 5.72 ± 0.37 mm), thoracic aorta (4.41 ± 0.55 mm), and carotid artery (2.06 ± 0.29 mm)), tracheae (15.05 ± 2.25 mm), pericardia, and esophagi (11.8 ± 0.91 mm) were harvested from three female beagles (age: 1 year). Rabbit tracheae (5.85 ± 0.20 mm) were harvested from three Japanese white rabbits (age: 3 months). Three glutaraldehyde-pretreated human pericardia (age: 73 years (male), 79 years (female), 85 years (male)) were supplied by Oita University after aortic valve reconstruction (i.e., Ozaki procedure) [3]. One bovine pericardium was purchased from Edwards Lifesciences (Irvine, CA, Model No. 4700, SN 4294581).

2.2.2.5 Measurements of wall thickness and lumen holding force

Wall thicknesses were measured using a thickness gauge (ID-C1012XBS, Mitsutoyo, Kanagawa, Japan). After immersion in physiological saline for 10 min, the ring-shaped samples (10-mm length) were compressed using a rheometer (RE2-33005C, Yamaden, Tokyo, Japan) with a flat plunger at a constant speed (0.1 mm/s) until the inner diameter ratio was reduced by 30%. The lumen holding force at 25% deformation was normalized by the following equation:

$$F_n = F \times {\left({\varphi_i}/{2}\right)^2}\Big/{L}$$

where F_n is the normalized lumen holding force; F, the lumen holding force; φ_i, the inner diameter of the tube; and L, the longitudinal-axis length of the tube.

2.2.2.6 Measurements of breaking strength and elastic modulus

Tissue strengths were measured using a tensile tester having a hemispherical plunger with a 5-mm diameter (P&M, Fukushima, Japan). The tissue samples, which were cut to form (10 × 10)-mm squares and then fixed to a sample folder, were stress-loaded to rupture at a rate of 0.05 mm/s. The breaking strength was defined as the maximum load value (gf) at the highest point of the load-extension curve. The ultimate elastic modulus (MPa) was determined from the maximum slope of the load-extension curve.

2.2.2.7 Histological examination

Biotubes were fixed with 10% neutral buffered formalin, embedded in paraffin, and sectioned into (3–5)-μm sections. The specimens were stained with hematoxylin and eosin stain for the general examination, Masson's trichrome stain for collagen testing, and Elastica van Gieson stain for elastin testing.

2.2.2.8 Statistical analysis

The results were expressed as mean ± standard deviation. The analysis of variance and t-test were used to check for significant differences among the groups, and $p < 0.05$ was considered significant. Linear relationships were examined by linear regression analysis.

2.2.3 Results

Large-sized Biotubes whose inner diameters were over 11 mm were formed in all the molds for every gap distance (Figure 2-2-1B). All Biotubes had almost the same

outer diameter of 19 mm, which corresponded to the inner diameter of the cage. Their wall thickness was approximately 1–3 mm and increased linearly with the gap distance; consequently, the Biotube tissues filled approximately 80% of the gap (Figure 2-2-1A). All the Biotubes were collagen-based tissues regardless of the wall thickness (Figure 2-2-1C a, b). Even at the center part of the thickest tissue, significant necrosis was not observed with many angiogenesis (Figure 2-2-1C c). At the outside of the wall, elastic fibers were observed near the slit parts (red arrowheads in Figure 2-2-1C d).

The mechanical properties of the Biotubes are summarized in Figure 2-2-2B–D. The breaking strength almost linearly increased with the wall thickness of the Biotubes (Figure 2-2-2B). Comparison of Biotubes and blood vessels compared with arteries that are close in thickness. The thinnest Biotubes were compared with the carotid artery, and no significant difference in breaking strength. The second and third thin Biotubes was compared with the thoracic aorta and ascending aorta, both of which were higher than that of beagle blood vessels. The thickest Biotubes were as strong as bovine pericardium. Young's modulus, which ranged from 1 to 3 MPa, exhibited only minor correspondence with the wall thickness and was similar to that of beagle pericardium (Figure 2-2-2C). The lumen holding force increased exponentially with the wall thickness (Figure 2-2-2D). The thickest Biotubes had similar holding force to rabbit trachea.

2.2.4 Discussion

The important requirements for graft materials used for tubular tissues are stress-withstanding ability, availability of various sizes for preparation, on immunogenic ability, and infection resistance. A tissue-engineering approach may have the potential to satisfy these requirements. However, the tissue fabricated by this approach has been

found to possess low breaking strength—approximately half that of the native blood vessel [4]. In general, the in vitro preparation of millimeter-scaled thick tissues is very difficult because of the limited supply of oxygen and nutrient agents (<~200 μm). Therefore, even in sheet-like tissues, vascularization is necessary for culturing. For example, cardiomyocyte sheets, which are formed using a temperature-responsive culture dish, are cultured in vitro using collagen gel and a vascular endothelial cell growth factor with the formation of vascularization, which requires complex facilities and processes [5]. Multiple transplantations of the cardiomyocyte sheets into a living body are repeatedly performed to form a vascular network in vivo for preparing thicker tissues of approximately 1 mm [6].

On the other hand, in this study, thick wall tissues with over 3-mm thickness were formed in vivo using the type-C mold within 3 months. The thickness could be controlled in the range of 1–3 mm. Numerous capillary vessels developed automatically with the growth of the tissues. Therefore, necrosis hardly occurred even in the millimeter-sized tissues. Even thicker tissues could be obtained by using the type-C mold. Previously, type-C Biotubes with an approximately 2-mm inner diameter and 1-mm wall thickness were implanted into beagle femoral arteries, resulting in perfect patency with little stenosis and no aneurysmal dilation in an acute phase model [2]. However, a large wall thickness was needed to strengthen the luminal structure, where a vascular network that supplied nutrition to the cells was to be created [7]. The breaking strength of all the Biotubes having a wall thickness of about 1.5 mm or more obtained in the present study was higher than that of beagle blood vessels. Therefore, it is expected that Biotubes with appropriate wall thickness can be used as beagle aortic grafts.

Biosheets, which are IBTA-based sheet-like tissues, were applied for patch

implantation in the reconstruction of the trachea [8] or esophagus [9]. The thickest Biotubes had a high breaking strength, and their lumen holding force was similar to that of rabbit trachea. Therefore, they may be used as a conduit implant in airway reconstruction, at least in rabbits. Actually Biosheets, which are IBTA-based sheet-like tissues, were already applied for patch implantation in the reconstruction of the trachea [8] or esophagus [9] in animal experiments.

2.2.5 Conclusion

The IBTA using the type-C mold was effective in the formation of large-diameter Biotubes with a large wall thickness of 1–3 mm. The thick Biotubes may be used as vascular grafts for large-diameter arteries such as the aorta and as alternative grafts for other tubular or sheet-like tissues such as tracheae, esophagi, or pericardia.

2.2.6 References

[1] Nakayama Y, Furukoshi M. Feasibility of in-body tissue architecture (IBTA) in pediatric cardiovascular surgery: Development of regenerative autologous tissues with growth potential. Pediatr Cardiol Card Surg. 2016;32:199–207.

[2] Furukoshi M, Moriwaki T, Nakayama Y. Development of an in vivo tissue-engineered vascular graft with designed wall thickness (biotube type C) based on a novel caged mold. J Artif Organs. 2016;19:54–61.

[3] Ozaki S, Kawase I, Yamashita H, Uchida S, Takatoh M, Hagiwara S, Kiyohara N. Aortic valve reconstruction using autologous pericardium for aortic stenosis. Circ J. 2015;79:1504–1510.

[4] Itoh M, Nakayama K, Noguchi R, Kamohara K, Furukawa K, Uchihashi K, Toda S, Oyama J, Node K, Morita S. Scaffold-free tubular tissues created by a Bio-3D printer undergo remodeling and endothelialization when implanted in rat aortae. PLoS ONE. 2015;10:e0136681.

[5] Shimizu T, Yamato M, Kikuchi A, Okano T. Two-dimensional manipulation of cardiac myocyte sheets utilizing temperature-responsive culture dishes augments the pulsatile amplitude. Tissue Eng. 2001;7:141–151.

[6] Shimizu T, Sekine H, Yang J, Isoi Y, Yamato M, Kikuchi A, Kobayashi E, Okano T. Polysurgery of cell sheet grafts overcomes diffusion limits to produce thick, vascularized myocardial tissues. FASEB J. 2006;20:708–710.

[7] Novosel EC, Kleinhans C, Kluger PJ. Vascularization is the key challenge in tissue engineering. Adv Drug Deliv. 2011;63:300–311.

[8] Satake R, Komura M, Komura H, Kodaka T, Terawaki K, Ikebukuro K, Komuro H, Yonekawa H, Hoshi K, Takato T, Nakayama Y. Patch tracheoplasty in body tissue engineering using collagenous connective tissue membranes (biosheets). J Pediatr Surg. 2016;51:244–248.

[9] Okuyama H, Umeda S, Takama Y, Terasawa T, Nakayama Y. Patch sophagoplasty using an in-body-tissue-engineered collagenous connective tissue membrane. J Pediatr Surg. 2018; 53: 223-226.

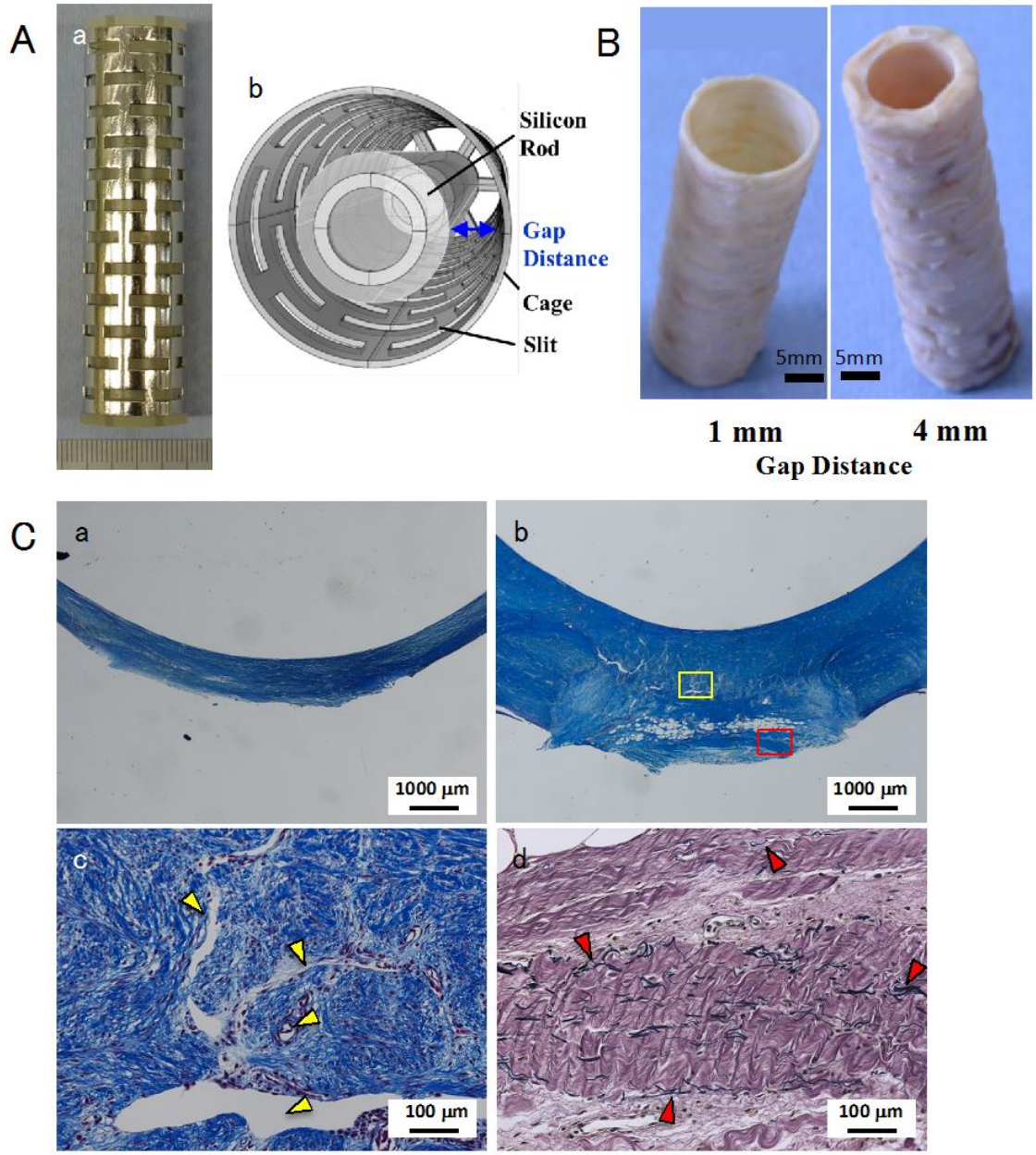

Figure 2-2-1. (**A**) (**a**) Photo of type-C mold assembled with silicone rod and cylindrical cage with slits. (**b**) Illustration of cross-sectional view of mold. The rod–cage gap distance is set by changing the outer diameter of the rod. (**B**) Photos of Biotubes formed with 1- or 4-mm gap distances. (**C**) Histological cross-sectional micrographs of Biotubes stained with Masson's trichrome stain for collagen testing (**a–c**), and with Elastica van Gieson for elastin testing (**d**). The gap distance is 1 mm in (**a**) and 4 mm in (**b–d**). **c** is an enlarged picture of the yellow rectangle part in **b**. **d** is an enlarged picture of the red rectangle part in **b**.

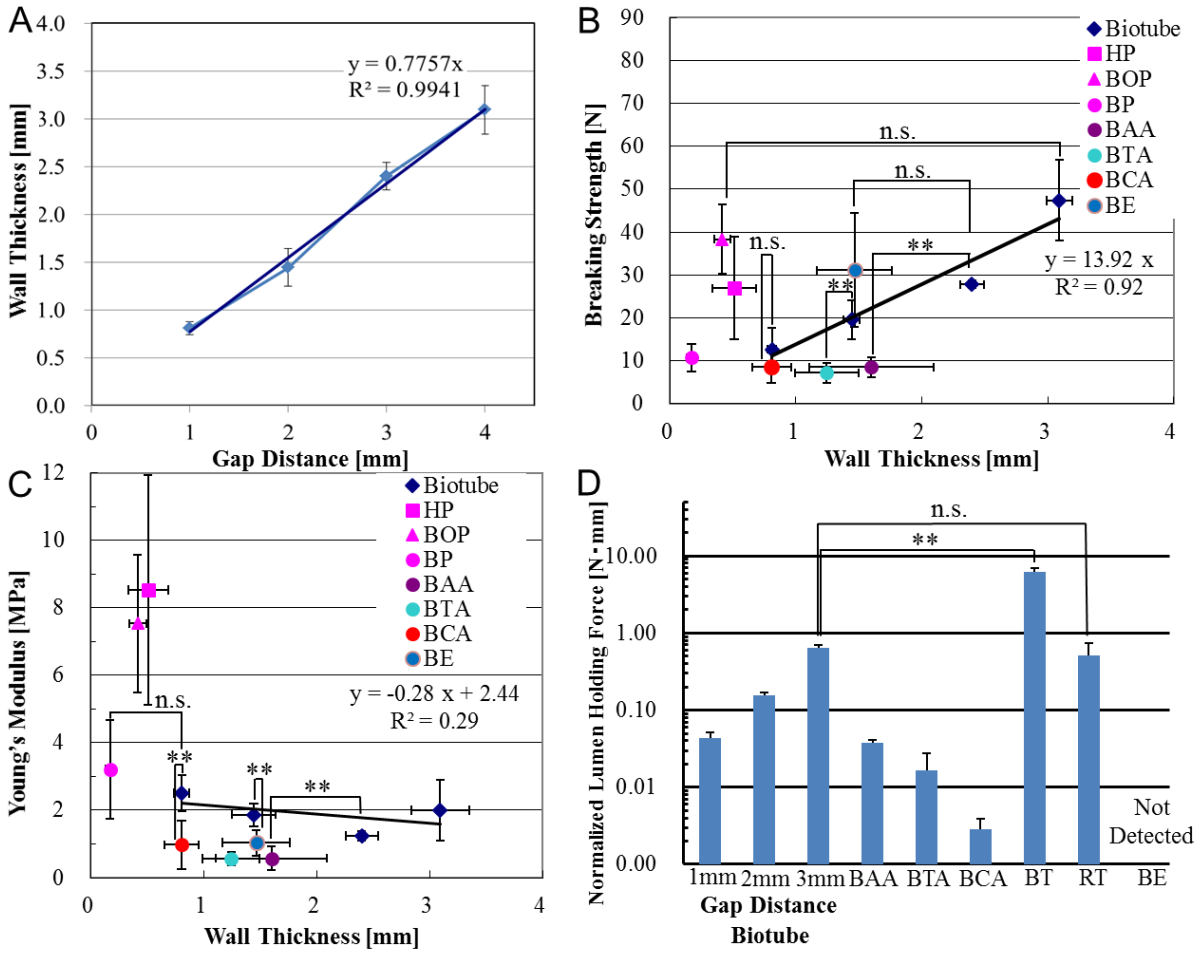

Figure 2-2-2. (**A**) Wall thickness of formed tissue relative to gap distance of mold. (**B**) Relationship between wall thickness and breaking strength, and comparison between Biotubes and native tissues. (**C**) Relationship between maximum Young's modulus and wall thickness. (**D**) Comparison of lumen holding force of Biotubes and native tissues. HP: Human pericardium, BOP: Bovine pericardium, BP: Beagle pericardium, BAA: Beagle ascending aorta, BTA: Beagle thoracic aorta, BCA: Beagle carotid artery, BT: Beagle trachea, RT: Rabbit trachea, BE: Beagle esophagus.

Chapter 2.3

Possibility to aortic valve reconstruction materials of iBTA-induced sheet-like tissues (Biosheets)

2.3.1 Introduction

Aortic valve replacement with a mechanical or biological prosthesis is a safe and established procedure, and regarded as being the gold standard in the treatment of aortic valve stenosis or regurgitation. However, mechanical valves are preferred for application in younger patients (< 60 years) because of their longer lifetime, while biological valves are used with elderly patients in order to avoid the need for oral anticoagulants. Ozaki et al. developed a method of aortic valve reconstruction using autologous pericardium for aortic valve neo-cuspidization (AVNeo) [1,2]. In this method, autologous pericardium is collected and then crosslinked with glutaraldehyde (GA) to form a material for application to aortic leaflets. The GA-treated pericardium was intraoperatively customized and tailored according to individual sinus measurements and based on appropriate Ozaki templates. The leaflet-shaped pericardium was sewn along the aortic annuli. In 850 patients treated using AVNeo for aortic stenosis (AS), satisfactory medium-term results were reported for durations of up to 118 months [1]. However, for young patients, there are concerns about there being an insufficient amount of pericardium available for any subsequent operation and

decreased coaptation due to growth; the durability of the autologous pericardium is also unknown.

Nakayama et al. previously developed autologous prosthetic tissues using in-body tissue architecture (iBTA) [3]. iBTA is a cell-free tissue-engineering technology that can produce autologous implantable collagenous tissues with a desired shape by the simple subcutaneous embedding of a specially designed mold. Biosheets, which are iBTA-induced membranous tissues, have been applied to the cornea [4], as well as to the repair of the diaphragm [5] and esophagus [6]. In the present study, I examined the material (thickness and density) and mechanical properties (ultimate tensile strength, fracture strain, and Young's modulus) of Biosheets. The possibility of adopting Biosheets as the leaflet material for AVNeo was discussed.

2.3.2 Materials and Methods

2.3.2.1 Ethical approval

All the animals used in this study received care according to the Principles of Laboratory Animal Care (National Institutes of Health, No. 56-23, received 1985), and the research protocols were approved by the Ethics Committee of the National Cerebral and Cardiovascular Center (No. 17013) and Oita University (No. 1622001). The clinical research process using human pericardium was approved by the Ethics Committee of the National Cerebral and Cardiovascular Center (No. M28-140) and by the Toho University Ohashi Ethics Committee (No.H16062).

2.3.2.2 Mold Preparation

The mold was assembled by inserting a silicone tube with an outer diameter of

15, 16, 16.3, or 16.5 mm into a stainless-steel pipe with an internal diameter of 18 mm (Figure 2-3-1a). Therefore, the gap constituting the tissue formation space between the silicone tube and the stainless-steel pipe was 0.75, 0.85, 1, or 1.5 mm, respectively. The stainless-steel pipe had many line slits arranged in one of two patterns; alternating or parallel (Figure 2-3-1b).

2.3.2.3 Preparation of Biosheet and human pericardia

The molds (n=30 with the alternating pattern, n=36 with the parallel pattern) were surgically embedded in the abdominal subcutaneous pouches of Saanen goats (n=12, 3–6 molds per goat, weight: 34–59 kg) under a combination of anesthetic induction by the intramuscular injection of ketamine and inhalation anesthesia with sevoflurane. After 7–12 weeks, the molds were harvested. The tubular tissues formed in the molds were removed and dried overnight. Biosheets (5×7 cm) were obtained by cutting the tubular tissues in the longitudinal direction and then storing them in a 70% ethanol solution prior to the measurements.

Human pericardia were used as a control (n=9, age: 33–68 years (male), 75–93 years (female)). The tissue, obtained from Toho University, was surplus remaining after AVNeo surgery and had been treated with 0.6% glutaraldehyde for 10 min.

2.3.2.4 Mapping of Biosheet thickness

Biosheet (n=29 (alternating pattern), n=33 (parallel pattern)) or human pericardia (n=9) samples were immersed in a saline solution for 10 min. Thickness mapping was performed over the entire surface by applying optical coherence tomography (OCT, IVS-2000, Santec, Aichi, Japan), as follows. The spatial resolution

of the OCT was 0.0391 mm (surface length) and 0.008 mm (depth). The sample was placed with its smooth surface in close contact with the stage, and laser light was irradiated perpendicularly onto the stage surface. An algorithm was developed to calculate the thickness distribution by determining the local maximum point of the reflection intensity closest to the depth direction from the irradiation position as the sample surface position. A histogram having a class of 0.008 mm was prepared from the obtained map, and the distribution of the area occupied by each thickness of the sheet was obtained. The total area was calculated by integrating the histogram for a given sheet thickness, and the volume was obtained by integrating the voxels.

2.3.2.5 Measurement of Biosheet density

The density of the Biosheet was calculated by dividing the sheet weight by the sheet volume.

2.3.2.6 Calculate of success rate of Biosheet formation

Presence or absence of the defects in the Biosheets were checked visually. The success rate of the Biosheets were calculated as the number of the Biosheets without defects per the total number of the Biosheets.

2.3.2.7 Measurement of ultimate tensile strength, elastic modulus, and breaking strength

The tissue strength was measured using a uniaxial tensile tester (EZ-LX, Shimadzu, Kyoto, Japan). Biosheets (n=20 (alternating pattern), n=36 (parallel pattern)) or human pericardia (n=18) were cut into a dumbbell shape (tensile region: 5 mm (W) ×

5 mm(L)) as a sample and then set between two chucks. The initial length of the samples was fixed by applying a preliminary load of 0.02 N. The stress was applied in the circumferential or longitudinal direction relative to the break at a rate of 0.5 mm/s. The breaking strength was defined as the maximum load (N) at the highest point of the obtained load-extension curve. The unit breaking strength was defined as a value obtained by dividing the breaking strength by the sample width. The true stress/true strain was calculated using the reported method [7]. The ultimate tensile strength was determined from the maximum value of the stress, while Young's modulus (MPa) was determined from the maximum slope of the stress–strain curve.

2.3.2.8 Statistical analysis

The results were expressed as a mean ± standard deviation. Analyses of the variance and t test were used to check for significant differences between the groups, with $p<0.01$ being considered significant. Linear relationships were examined by regression analysis.

2.3.3 Results

2.3.3.1 Thickness of Biosheets

Biosheets were obtained as thin white sheets with either alternating or parallel slit patterns, depending on the type of the cylindrical mold (Figure 2-3-1b). The success rate of the Biosheet production when using the alternating-pattern mold was 96.7%, while that for those produced with the parallel mold was 97.2%. Figure 2-3-1c shows the two kinds of Biosheets obtained by drying and storing in an alcohol solution as a post-treatment after tissue harvesting. All the Biosheets exhibited extremely flat

surfaces at the face in contact with the silicone, and a convex surface with line projections corresponding to the slits in the stainless-steel pipe.

Figure 2-3-1d shows typical examples of the color mapping of the thickness distribution of the two kinds of Biosheets. For both Biosheets, the surface without the line projection portions was smooth without any defects such as pinholes. The thickness was almost uniform in the horizontal direction corresponding to the longitudinal direction in the cylindrical mold, as shown in Figure 2-3-1d, but in the vertical direction periodically changed to the circumferential direction. The change frequency was 1 Hz for the alternating slit pattern, and 2 Hz for the parallel one, and was not dependent on the size of the gap in the mold. The thickness of the Biosheet obtained from the mold with a 1-mm gap ranged from ca. 0.1–0.8 mm, being mainly distributed in the 0.2–0.5 mm range (Figure 2-3-1e). The average wall thickness was almost the same for both types of Biosheet (0.32 ± 0.05 mm for the alternating slit pattern and 0.36 ± 0.10 mm for the parallel type). Regardless of the slit pattern, the average wall thickness was controlled from ca. 0.2–0.5 mm by varying the size of the gap (0.75–1.5 mm) in the molds, which corresponded to ca. 30% of the size of the gap (Figure 2-3-2).

2.3.3.2 Density of Biosheets

The relationship between the thickness and density of the Biosheets is summarized in Figure 2-3-3. The density decreased with the thickness for both slit patterns (Figure 2-3-3a,b), indicating that the wall of the Biosheet was on-homogeneous in depth and the low-density component increased with the thickness. For any given thickness, the Biosheets obtained from those molds with a larger gap had a lower density, especially those derived from the parallel-patterned molds. The distribution of

the thickness and density for each individual goat is shown in Figure 2-3-3c,d. For any one mold, the resulting tissues were almost the same in a given individual, but differed between individuals. Thus, I can say that the variation in Biosheet formation was minimal within individuals, but significant between individuals.

2.3.3.3 Mechanical properties of Biosheets

The mechanical properties of the Biosheets obtained with the alternating and parallel slit-pattern molds were examined by undertaking a tensile test in their circumferential and longitudinal directions (Figure 2-3-4). For those Biosheets obtained from the alternating-pattern molds, there was no significant difference in their mechanical properties (ultimate tensile strength, fracture strain, and Young's modulus) regardless of the tensile direction and gap distance (Figure 2-3-4A). On the other hand, for those Biosheets produced from the parallel-pattern molds, a significantly large ultimate tensile strength and Young's modulus were obtained in the longitudinal direction corresponding to the direction of the slits. And in any of the evaluation indices, there was no difference depending on the gap distance of the mold between each tensile direction (Figure 2-3-4B).

The relationship between the mechanical properties and density of the Biosheets is shown in Figure 2-3-5 which is mixed both circumferential and longitudinal axis sample. The ultimate tensile strength increases with the density for all the Biosheets (Figure 2-3-5a). There was no correlation between the strain and the density. The Young's modulus increased with density for both types of molds. The parallel pattern Biosheets had large error bar compared to the alternating pattern Biosheets.

The results of comparing the unit breaking strength of the Biosheets obtained

from the alternating pattern mold with GA-treated human pericardium and human valve leaflets are shown in Figure 2-3-6. The force that could be applied to the Biosheets tended to increase almost linearly with the thickness, giving a slope of 10.32 N/mm^2. The force that could be applied to the thinnest Biosheet, with a thickness of 0.267 mm, was 2.04 N/mm. The strength of the human pericardium also tended to increase almost linearly with its thickness. The slope of the correlation was about twice as steep as that for the Biosheets. However, the thickness distribution of the pericardium ranged from ca. 0.1–0.35 mm, such that the force that could be applied was widely distributed from 0.7 N/mm. The thickness of the Biosheets and the force that they could withstand were higher than the minimum value of human pericardium, given that the ultimate tensile strength of human leaflet is about 2 MPa [8] and the thickness of the valve leaflet is reported as being 0.44 mm in the thickest part [9]. Therefore, the unit breaking strength was calculated to be 1.0 N/mm, which was much lower than that of any of the Biosheets.

2.3.4 Discussion

I focused on the material and physical properties of the Biosheets to clarify whether their properties and strength are sufficient to allow their application to AVNeo aortic valve reconstruction surgery. In order to investigate the influence of the directionality of the slits of the tissue formation and on the anisotropy mechanical strength in the Biosheets, I designed the two different slit types of molds. An almost perfect Biosheet preparation success rate was obtained regardless of the slit patterns. To avoid stress concentration, a sheet material should be homogenous and have a constant thickness. The Biosheets had one flat surface and another convex surface with multiple

line projections corresponding to the slits in the stainless-steel pipes of both molds. The slits act as entrances for the fibroblasts. The cells penetrate the slits and enter the gap inside the molds to produce collagen, thus forming the Biosheets. Therefore, the presence of the slits, although disadvantageous in some respects, is essential to the preparation of the Biosheets. However, the entire surface of each Biosheet, except for the line projections, was very smooth and exhibited no defects.

The average thickness of the formed Biosheets increased with the mold gap. This tendency was very similar to that observed in our previous study using cows, where the wall thickness of the formed tissues was ca. 1–3 mm, which corresponded to approximately 80% of the gap.[10] In the present study, the thickness of the Biosheets after drying was about 35% of the gap, even after immersion in physiological saline. Therefore, the Biosheets were compressed to about 40% by drying. Therefore, I can conclude that the Biosheets can be thinned simply by drying.

Both types of mold exhibited variations in their thickness in the circumferential direction, but not along their long axis. The change frequency was 1 Hz for the alternating slit pattern, and 2 Hz for the parallel one. For the alternating pattern, it was thought that the thickness change depended on the deviation from the absolute center of the central rod as by pressure received from the skin. In the parallel pattern, in addition to the misalignment of the center rod, deformation of the pipe due to the lower lumen retention than the alternating pattern was also a factor. It should be possible to resolve this problem by improving the design of the structure to make it less susceptible to subcutaneous pressure, by improving the accuracy of the centering of the mold, or by using rigid material.

The difference in the slit type induced anisotropy in the physical properties. With

the alternating pattern, little anisotropy in the ultimate tensile strength was observed, and the variation of it was mainly the difference in density depending on the thickness and the individual difference. But with the parallel pattern, the ultimate tensile strength was higher in the direction of the slit lines rather than density or individual differnce. Given that the presence of the slits gave rise to projections on the Biosheets, it is possible that the physical properties could be controlled by adjusting the slit shape (direction and size). Since the two types of molds used in this study differ in their aperture ratio and opening area, it is unclear which parameter is affected. I will seek to clarify this point in our future work.

Considering the usability of the Biosheets, it would be better to be able to cut as leaflets in any direction. The Biosheets from the alternating-pattern had low anisotropy. Therefore, I selected the alternating-pattened Biosheets as a candidate material for the substitution of the aortic leaflets. The slope of the unit breaking strength indicates that the physical strength of the alternating-patterned Biosheet is stronger than that of the leaflet, but weaker than that of clinically used human pericardium. This is probably because the pericardium is treated with glutaraldehyde (GA). However, since the actual strength depends on the thickness, the thicker Biosheet is stronger than the thinnest pericardium and has sufficient strength. Because the pericardium is thin, it is necessary to improve its physical strength through chemical treatment such as GA treatment but, on the other hand, the literature states that this is a result of calcification.[11] Since the thickness of the Biosheet can be tailored by adjusting the size of the gap, the strength could be enhanced by increasing the thickness without GA treatment, so Biosheet may have possibility to suppress the calcification. I am planning to investigate the presence or absence of calcification in the implantation experiments undergoing.

Decellularized tissues are GA-free and, as such, are a popular choice for implantation. SynerGraft, which is a decellularized porcine aortic valve, is a commercial pulmonary valve.[12] When a decellularized pericardial patch was used in a tri-leaflet aortic valve reconstruction in a sheep model, calcification was observed in 8 of 9 leaflets.[13] Recently, aortic valve conduits have been fabricated by using 3D bioprinting, but their performance in vivo is unknown.[14] One of the most important features of iBTA-induced tissue is its ability to regenerate. Upon the implantation of a valve-conduit Biovalve in the pulmonary valve position for 19 months, the cells constituting the leaflet gradually migrated and ultimately formed characteristic three-layered tissue without calcification, in the same way as the native leaflets.[15] Implanted Biovalves can adapt their histological structure according to their environment. They offer the potential to be used as viable grafts that better maintain their function and biocompatibility. An iBTA-Biosheet can be expected to grow through regeneration in the same way as a Biotube.[3] If it could be applied as a pediatric valvular leaflet, it would be possible to develop a revolutionary curative technique requiring no subsequent reoperations.

2.3.5 Conclusion

Thin and homogeneous Biosheets were prepared through the subcutaneous embedding of alternating slit pattern molds by using iBTA. The resulting Biosheets had no tiny defects and could be produced with an extremely high success rate. All the resulting Biosheets exhibited adequate mechanical strength regardless of their thickness, especially when compared to the GA-treated human pericardium used in AVNeo, which exhibited an extremely wide variation in strength. Even the weakest of the fabricated

Biosheets was stronger than the human aortic valve leaflets. Therefore, the alternately patterned Biosheets have sufficient strength for use in AVNeo. I have already started studies of AVNeo implantation using autologous Biosheets in a goat model. I expect to report on the results of this study in the near future.

2.3.6 References

[1] Ozaki S, Kawase I, Yamashita H, Uchida S, Takatoh M, Kiyohara N. Midterm outcomes after aortic valve neocuspidization with glutaraldehyde-treated autologous pericardium. J Thorac Cardiovasc Surg, in press.

[2] Yamamoto Y, Iino K, Shintani Y, Kato H, Kimura K, Watanabe G, Takemura H. Comparison of aortic annulus dimension after aortic valve neocuspidization with valve replacement and normal valve. Semin Thorac Cardiovasc Surg. 2017; 29: 143-149.

[3] Nakayama Y, Furukoshi M, Feasibility of In-body Tissue Architecture in Pediatric Cardiovascular Surgery: Development of Regenerative Autologous Tissues with Growth Potential. J Pediatr Cardiol Card Surg 2018; 2: 1-9.

[4] Takiyama N, Mizuno T, Iwai R, Uechi M, Nakayama Y, In-body tissue-engineered collagenous connective tissue membranes (BIOSHEETs) for potential corneal stromal substitution. J Tissue Eng Regen Med 2016; 10: E518-E526.

[5] Suzuki K, Komura M, Terawaki K, Kodaka T, Gohara T, Komura H, Nakayama Y, Engineering and repair of diaphragm using biosheet (a collagenous connective tissue membrane) in rabbits. J Perdiatr Surg 2018; 53: 330-334.

[6] Okuyama H, Umeda S, Takama Y, Terazawa T, Nakayama Y, Patch esophagoplasty using an in-body-tissue-engineered collagenous connective tissue membrane. J Perdiatr Surg 2018; 53: 223-226.

[7] Duprey A, Khanafer K, Schlicht M, Avril S, Williams D, Berguer R. In vitro characterisation of physiological and maximum elastic modulus of ascending thoracic aortic aneurysms using uniaxial tensile testing. Eur J Vasc Endovasc Surg 2010; 39: 700-707.

[8] Yamashita H, Ozaki S, Iwasaki K, Kawase I, Nozawa Y, Umezu M. Tensile Strength of Human Pericardium Treated with Glutaraldehyde. Ann Thorac Cardiovasc Surg 2012; 18: 434-437.

[9] Sahasakul Y, Edwards W, Naessens J, Tajik A. Age-related changes in aortic and mitral valve thickness: Implications for two-dimensional echocardiography based on an autopsy study of 200 normal human hearts. Am J Cardiol 1988; 62: 424-430.

[10] Terazawa T, Nishimura T, Mitani T, Ichii O, Ikeda T, Kosenda K, Tatsumi E, Nakayama Y, Wall thickness control in biotubes prepared using type-C mold. J Artif Organs, 2018; 21: 387-391.

[11] Schoen FJ, Levy RJ. Calcification of tissue heart valve substitutes: progress toward understanding and prevention. Ann Thorac Surg 2005; 79: 1072-1080.

[12] O'Brien MF, Goldstein S, Walsh S, Black KS, Elkins R, Clarke D. The SynerGraft valve: a new acellular (nonglutaraldehyde-fixed) tissue heart valve for autologous recellularization first experimental studies before clinical implantation. Semin Thorac Cardiovasc Surg. 1999; 11(4 Suppl 1): 194-200.

[13] Meuris B, Ozaki S, Neethling W, De Vleeschauwer S, Verbeken E, Rhodes D, Verbrugghe P, Strange G. Trileaflet aortic valve reconstruction with a decellularized pericardial patch in a sheep model. J Thorac Cardiovasc Surg 2016; 152: 1167-1174.

[14] Duan B, Hockday LA, Kang KH, et al.: 3D Bioprinting of Heterogeneous Aortic Valve Conduits with Alginate/Gelatin Hydrogels. J Biomed Mater Res A, 101:1255-1264,2013.

[15] Takewa Y, Sumikura H, Kishimoto S, Naito N, Iizuka K, Akiyama D, Iwai R, Tatsumi E, Nakayama Y. Implanted In-Body Tissue-Engineered Heart Valve Can Adapt the Histological Structure to the Environment. ASAIO J, in press.

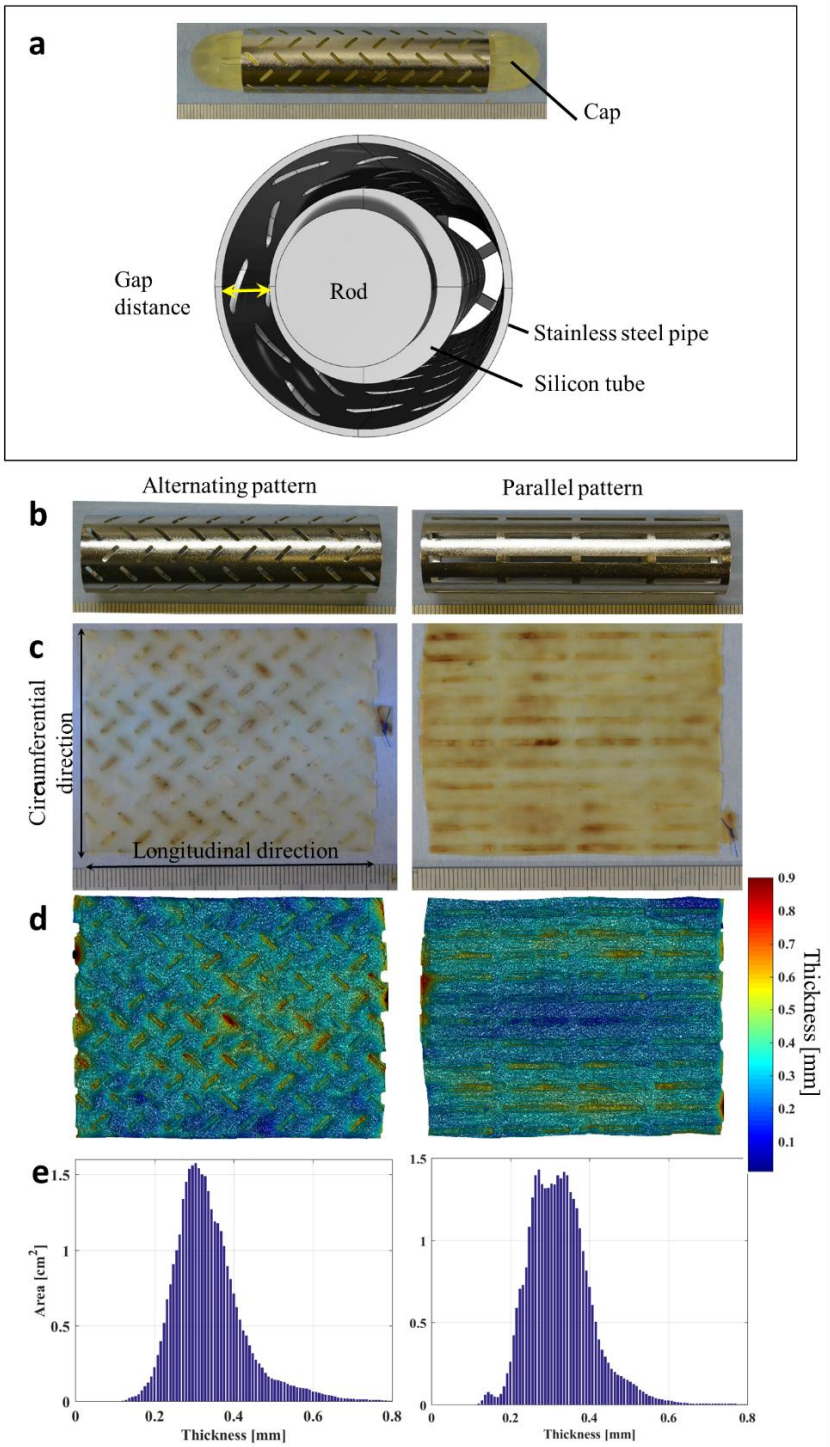

Figure 2-3-1. (a) Photo and cross-sectional illustration of the mold assembled from silicone tube and stainless-steel pipe with alternating line slits. (b) Photos of two types of pipes used for the molds, that is, with an alternating line pattern and a parallel pattern, and photos (c), thickness mappings (d), and thickness histograms of Biosheets obtained from each mold with a gap of 1 mm.

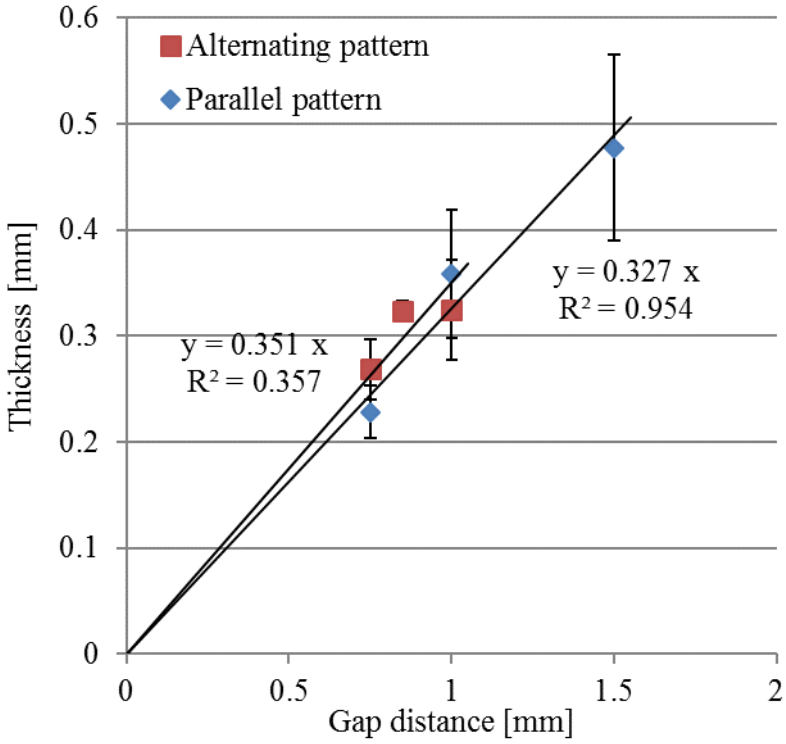

Figure 2-3-2. Relationship between gap and average wall thickness for both types of Biosheet.

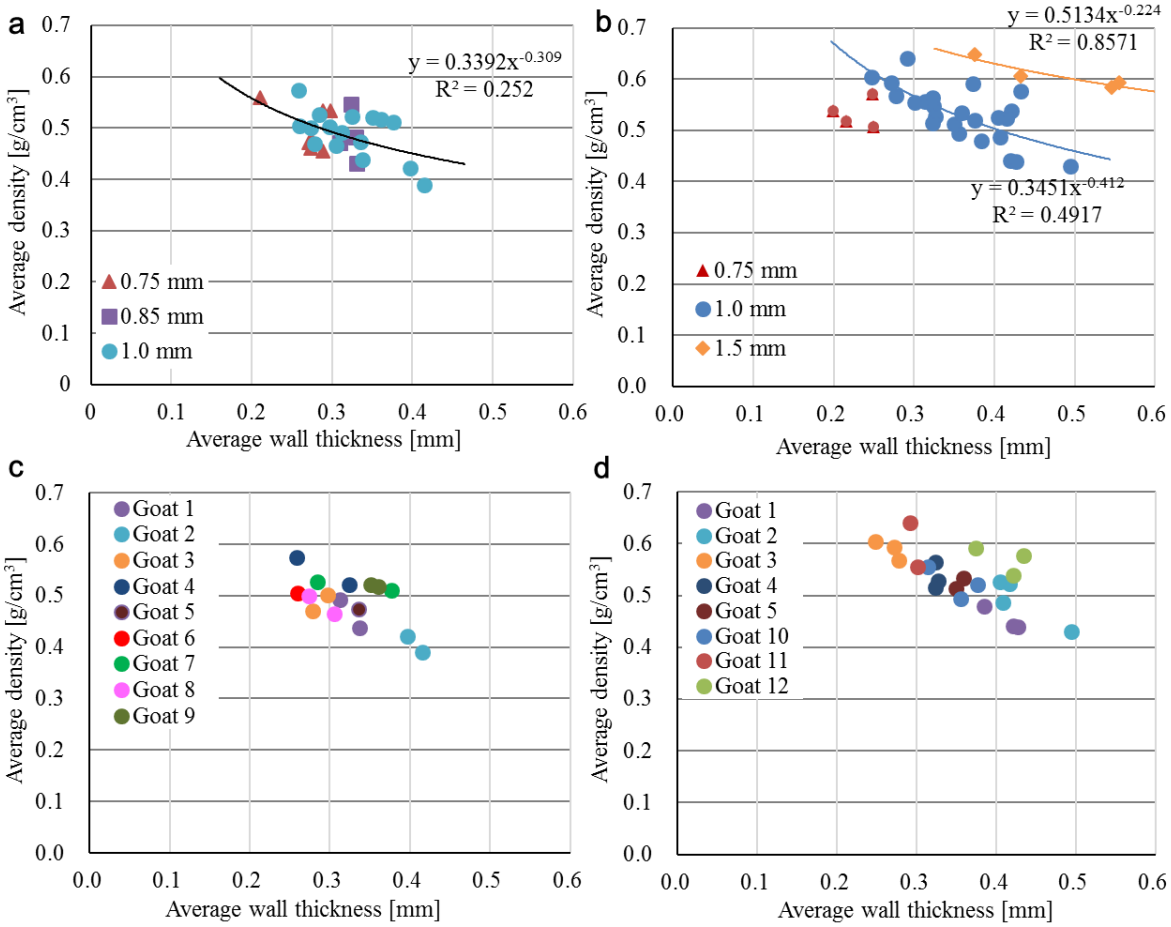

Figure 2-3-3. Relationship between average wall thicknesses of Biosheets with alternating slit pattern (a) or parallel slit pattern (b), and average density. (c) Relationship between average wall thickness of alternating-pattern Biosheet with gap distance 1 mm and average density for each goat. (d) Relationship between average wall thickness of parallel-pattern Biosheets with gap distance 1 mm and average density for each goat.

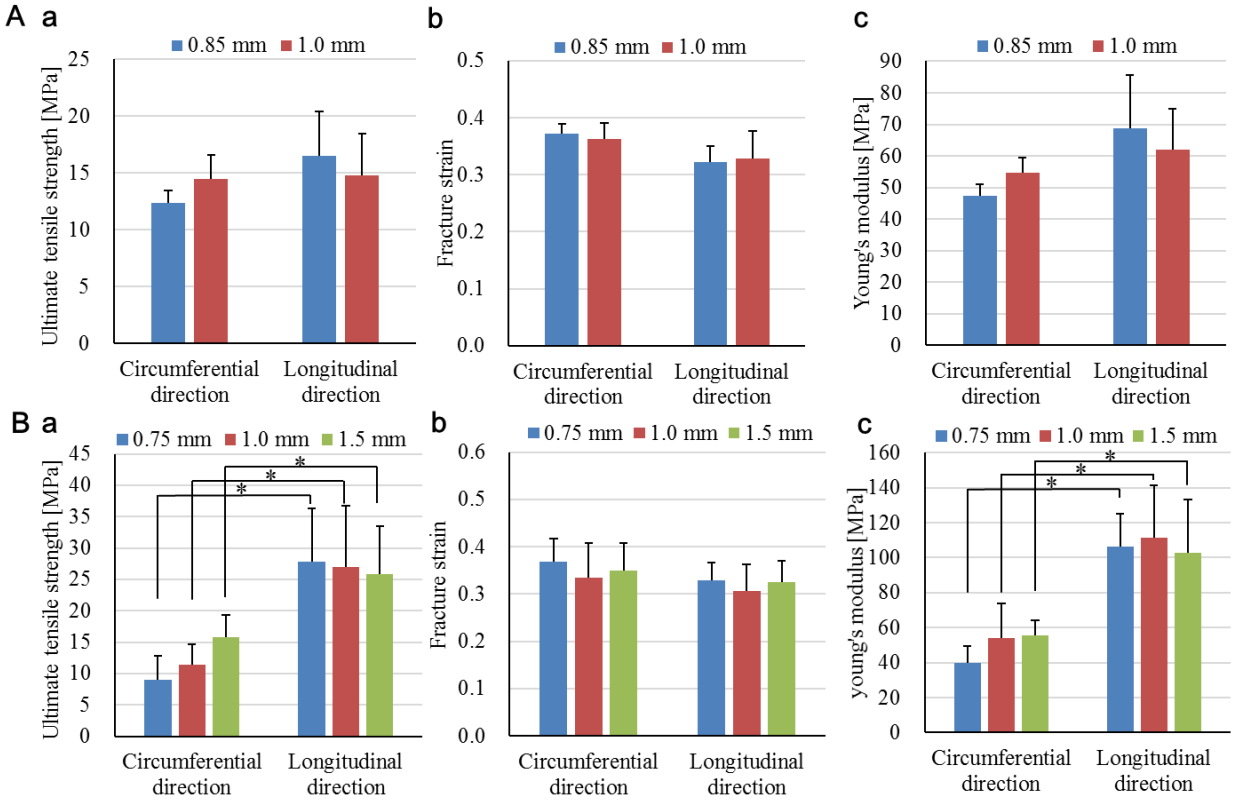

Figure 2-3-4. Ultimate tensile strength (a), fracture strain (b), and Young's modulus (c) of alternating-pattern Biosheets (A) and parallel-pattern Biosheets (B) in two directions (circumferential or longitudinal direction) are shown for each gap distance of the mold.

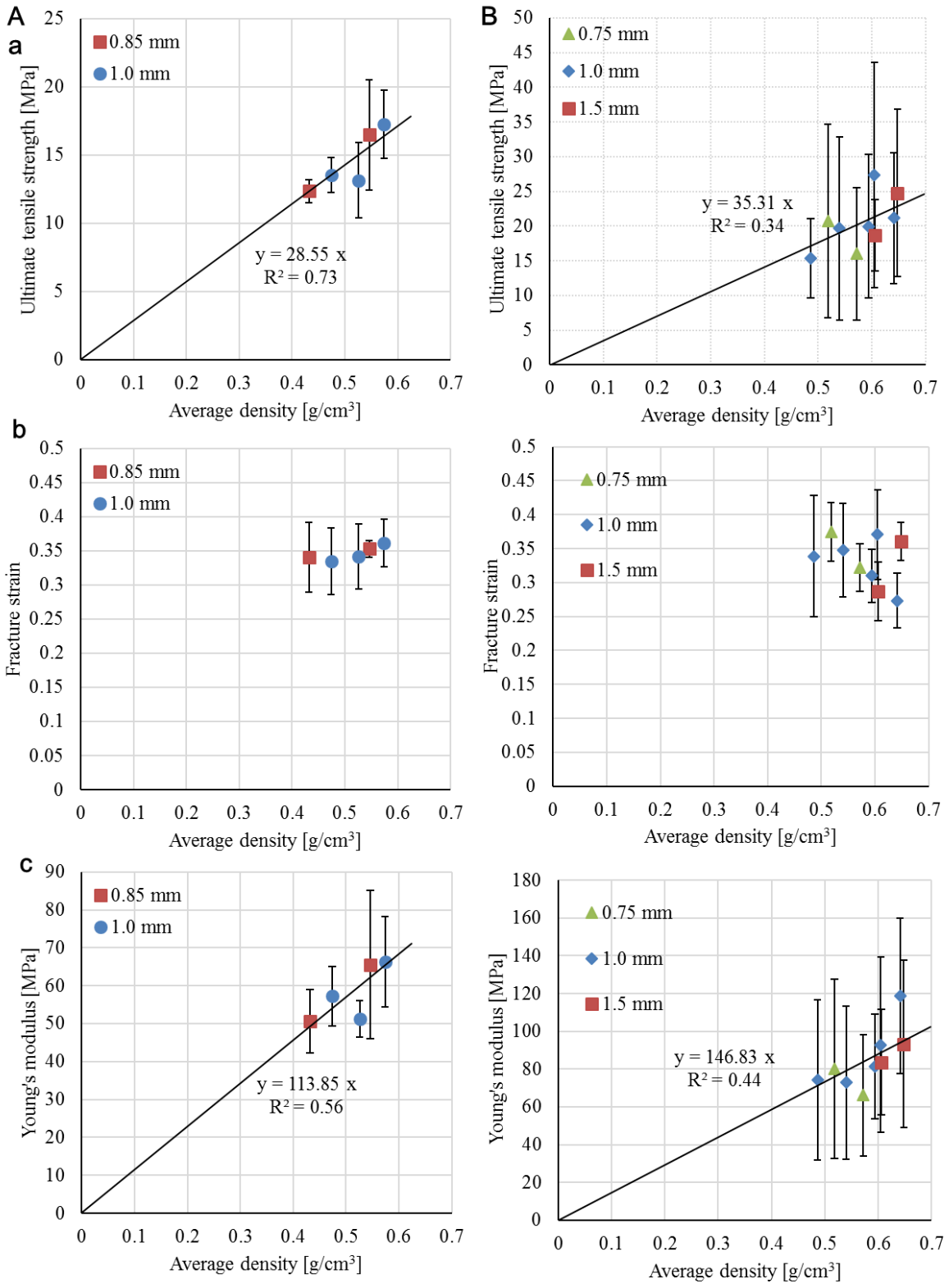

Figure 2-3-5. Relationships between average density and ultimate tensile strength (a), fracture strain (b), or Young's modulus (c) of alternating-pattern Biosheets (A) and parallel-pattern Biosheets (B).

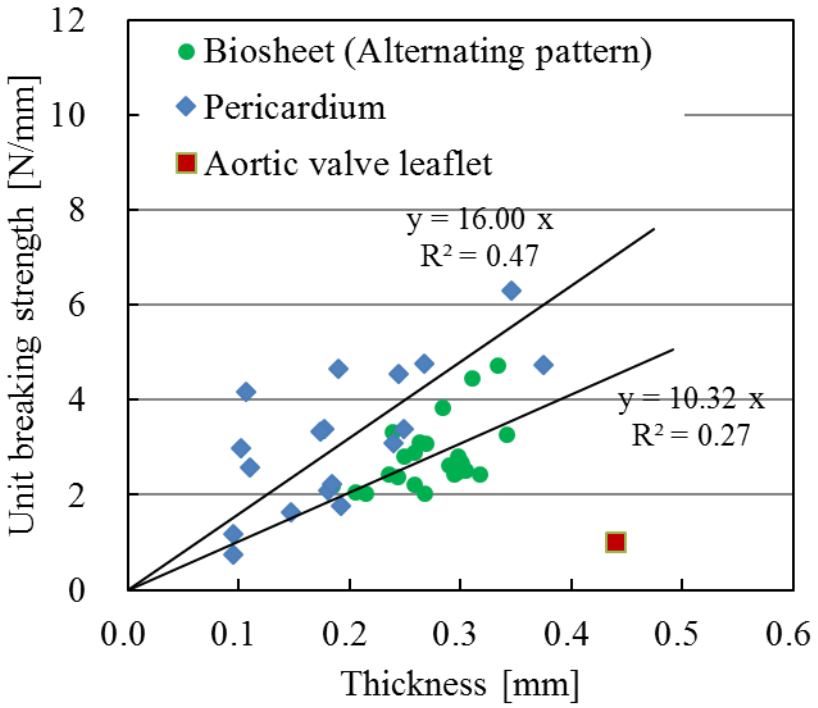

Figure 2-3-6. Relationship between unit breaking strength and thickness of alternating-pattern Biosheets, human pericardium after GA treatment, and human aortic valve leaflet.

Chapter 3

In-situ mechanical adaptation of iBTA-induced tissues after animal implantations

Chapter 3.1

Acute phase evaluation of Biosheets after implantation to beagle diaphragms

3.1.1 Introduction

Congenital diaphragmatic hernia (CDH) is the cause of severe dyspnea in newborns and has high mortality and occurs in about 1 in 2,000 to 3000 births [1, 2]. The CDH may be asymptomatic until adulthood, but depending on the site and extent of the defect, it may even lead to death immediately after birth [3]. Diaphragmatic hernia also occurs when a strong impact is applied to the abdomen during a traffic accident [4].

A defect can be healed in several ways. If the defect is small, the suturing method is effective; however, in case of a large defect (>5 cm), the hernia can relapse, so patch restoration is desirable [5, 6]. Artificial materials such as expanded polytetrafluoroethylene (ePTFE) and polypropylene are widely used as patch materials [7, 8]. However, because these patches are vulnerable to infection, recurrence of hernia and small intestinal obstruction may occur [9, 10]. In addition, ePTFE can cause chest wall deformation in fully obese patients with diaphragm, as growth does not accompany infant growth since ePTFE does not change in size at the time of implantation, chest wall deformation may occur with infant growth [11, 12].

Recently, sheet formation by tissue engineering methods such as cell sheet

engineering or Bio 3D printers has been realized [13]. Since these methods can form tissues based on certain cells, inflammatory reactions do not occur and high biocompatibility is realized. However, because it is difficult to artificially fabricate a capillary network, thick tissue formation has not been realized by these methods [14].

Furukoshi et al. have previously developed autologous prosthetic tissues using in-body tissue architecture (iBTA) [15], which is a cell-free tissue engineering technology that can produce autologous implantable tissues with a desired shape by simple subcutaneous embedding of a specially designed mold. Tissues developed with the iBTA technique include sheet-shaped Biosheets. In our previous study, Biosheets were successfully implanted as allogeneic substitutes in the corneal stroma in a rabbit model, and sufficient biological stability and biocompatibility were observed. In addition, Biosheets have been applied to a leaflet material for aortic valve neo-cuspidization (Ozaki method) [16]. Recently, Nakayama et al. reported that bovine Biosheets could be useful as off-the-shelf materials, where the Biosheets functioned as an abdominal wall repair material even in xeno-implantation in mid-term histological observation.

In this study, the mechanical change in allogenic Biosheets after implantation to beagle diaphragm defects within 3 months was examined for the evaluation of the availability of Biosheets as a hernia repair material for the diaphragm, with repeated powerful dynamic loading.

3.1.2 Materials and Methods

3.1.2.1 Ethical Approval

All animal experiments were performed according to the Guide for the Care

and Use of Laboratory Animals (United States National Institutes of Health, No. 85-23, received 1996), and the research protocols were approved by the ethics committee of Osaka Prefecture University (No.30-68).

3.1.2.2 Preparation of Biosheets

Biosheets were prepared according to our previous report [17]. Briefly, beagle dogs (body weight 7.8–9.5 kg) were administered atropine sulfate (0.025 mg/kg subcutaneously), butorphanol (0.2 mg/kg IV), midazolam (0.2 mg/kg IV), and cefovecin sodium (8 mg/kg IV). Anesthesia was induced with propofol (8 mg/kg IV) and maintained with 2% isoflurane. The molds were subcutaneously embedded in the beagles for 8 weeks. The tubular tissues were extracted from harvested molds, and then cut along their longitudinal direction to obtain Biosheets (Figure 3-1-1a). The Biosheets were stored in a 70% ethanol solution at room temperature prior to implantation.

3.1.2.3 Implantation of Biosheets

Under the same anesthesia as mentioned above the diaphragm of beagle dogs was approached through a midline abdominal incision in the supine position. The center of diaphragm including the whole tendon and muscle part was incised and a 6 cm × 4 cm defect was created. Biosheets, rinsed with saline at least 10 min before implantation, were sutured to the edge of the defect using a simple continuous suture with 3-0 polydioxanone (Figure 3-1-1b). The omentum was then covered over the Biosheets before the abdominal incisions were routinely closed in three layers. Biosheets were harvested 1 or 3 months after implantation, and then cryopreserved before mechanical experiments (Figure 3-1-1c).

3.1.2.4 Measurement of tensile strength

Before and after Biosheet implantation, the beagle diaphragm was immersed in physiological saline for at least 10 min. The extra tissues attached to the implanted Biosheet was removed carefully. The Biosheet samples were cut in dumbbell shape (tensile area 5 mm × 5 mm) to be oriented in the dorsal-ventral direction Y (n = 3 in pre-implantation, n = 11 in post-implantation, n = 10 in beagle diaphragm) and orthogonal direction X (n = 3 in pre-implantation, n = 12 in post-implantation, n = 10 in beagle diaphragm). The thickness of the sample before tensile loading was measured by performing optical coherence tomography (OCT, IVS-2000, Santec, Aichi, Japan). The spatial resolution of the OCT was 0.0391 mm in the surface direction, and 0.008 mm along the depth. The tensile strength was measured by using a uniaxial tensile tester (EZ-LX, Shimadzu, Kyoto, Japan). The distance between the end of the chucks of the tester was set to 5 mm, and the sample was fixed to them. Then, in order to exclude the initial deflection of the sample, a load of 0.02 N was applied to determine the initial sample length. The load was applied at a speed of 0.5 mm/s until rapture. The breaking strength was defined as the maximum load value (N) at the highest point of the obtained load-extension curve.

3.1.2.5 Calculation of mechanical characteristic value

The unit breaking strength was defined as the value obtained by dividing the breaking strength by the sample width. Elasticity was calculated as the spring coefficient calculated as the differential value of the load-extension curve. The load-extension curve was also fitted by the least squares method using the bilinear

model used in a previous study [18, 19]. The spring coefficient (toe region) was defined as the smaller one of the slopes of two straight lines that were regression coefficients of the bilinear model. True stress/true strain was calculated by the reported method [20], using the thickness of the breaking position previously measured with OCT, and the load and displacement measured with the tensile tester. The ultimate tensile strength (MPa) was determined from the maximum stress value, and the maximum Young's modulus (MPa) was determined from the maximum slope of the stress–strain curve. Stress–strain curves were also fitted with a bilinear model. The Young's modulus (toe region) was defined as the smaller one of the slopes of two straight lines that were regression coefficients of the bilinear model.

3.1.2.6 Statistical analysis

The results were expressed as mean ± standard deviation. Differences in mean values between groups were examined using the t test and $p < 0.05$ was considered significant.

3.1.3 Results

The stress–strain curve of the original Biosheets before implantation is shown in Figure 3-1-2. Stress gradually increased with strain and the shape of the curve became concave up. The straight lines obtained by bilinear fitting by the least squares method are superimposed in the figure. The strain at the intersection of the bilinear line is the transition strain, the strain region smaller than that is the toe region, and the larger strain region is the linear region. The tendencies observed in the implanted Biosheets and native diaphragm tissues were similar. From the stress–strain curves, five

representative physical indicators, namely, the ultimate tensile strength, fracture strain, Young's modulus at the toe region, maximum Young's modulus, and linear transitional strain at the toe region, were calculated. Upon comparing all the mechanical values in two orthogonal directions of the Biosheets before and after implantation, and native diaphragms, slight anisotropy was observed (Figure 3-1-3). In the native diaphragms. the tendon part had a large area and was responsible for the mechanical strength.

Since the directional dependence of each tissue was not identified (Figure 3-1-3), data corresponding to both directions were obtained together; the mechanical properties corresponding to the implantation period are summarized in Figure 3-1-4. The thickness of the Biosheets increased to about 1.5 mm (about three times that of the original Biosheets) within 1 month of implantation, and this thickness was maintained for 3 months, which was about three times as the tendon tissue. Actual strength (unit breaking strength) of the Biosheets increased significantly in 1 month and became almost the same as the diaphragm tendon part. The actual elasticity of the toe area (spring coefficient) was not changed by implantation, which was equivalent to the elasticity of the diaphragm tendon. On the other hand, the maximum actual elasticity (maximum spring coefficient) showed a 2.5-times increase in 1 month after implantation, to the same value as Tendon part.

Further, the significant low material-specific strength (ultimate tensile strength) of Biosheets, which was about 1/5 of that of the native diaphragms, hardly change as a result of implantation. Moreover, little change is observed in the low fracture strain of Biosheets because of implantation.

The maximum Young's modulus also tends to approach the native diaphragm value after implantation, but no significant change was observed, which was about half

of that of the native diaphragm. On the other hand, both the Young's modulus in the toe region and the transition strain, changed significantly. The Young's modulus of the toe region of the pre-implant Biosheet and that of the native diaphragm showed no significant difference, but after implantation, the difference between Biosheet and native value is increased, and a significant decrease was observed 3 months after the implantation: it was about 1/4 of the native diaphragm value. The transition strain of the Biosheet before the implantation was significantly smaller than that of the native diaphragm, but it increased significantly at 1 month after implantation and remained the same at 3 months after the implantation, it corresponded to the native diaphragm value.

3.1.4 Discussion

In this study, I focused on the strength and elasticity to investigate whether the Biosheet has adequate mechanical properties as a graft material to the diaphragm. The pre-implantation Biosheet showed a unit breaking strength of about 40% with respect to the tendon tissue, and the actual strength was lower than that of the native tissue. However, the Biosheet did not rupture after implantation, one month passed and it had changed to strength corresponding to the beagle’s tendon of diaphragm. Even at 3 months after the implantation, the unit breaking strength was equivalent to that after 1 month, and it seemed to approach the native tissue strength value. The unit breaking strength representing the actual strength is expressed by the following equation: $Fu = \sigma b \times t$. Here, σb is the ultimate tensile strength representing material characteristics, and t is the tissue thickness. The ultimate tensile strength of the Biosheet did not change even after implantation. On the other hand, the thickness of the Biosheet implantation section dynamically changed to 2.6 times as thick as 1 month after implantation. The thickness

was maintained even 3 months after implantation. Further, a new tissue was formed on the surface of the Biosheet tissue. Since the ultimate tensile strength of the after implantation Biosheet is equivalent to that before implantation, it is considered that tissue with material properties similar to those of the Biosheet was formed on its surface. Thus, there may be a mechanism for feedback regulation in order to maintain tissue strength at restoration (Figure 3-1-5). Actual diaphragm tension may be inferred from consecutive cells and there may be a mechanism by which the actual intensity is adjusted to be sufficient. In a short period of at least about a month, the Biosheet seems to promote the migration of cells involved in repair by functioning as a scaffold to form tissue. In order to improve the actual strength, it is imperative that it may be more efficient to thicken the tissue itself rather than to rebuild a dense tissue while decomposing the Biosheet.

The strength of the human diaphragm has been reported [4]. Based on this report, the unit breaking strength was calculated to be 3.67 ± 2.43 (N/mm). This value is larger than that of the Biosheet before implantation (2.3 ± 1.1 (N/mm)), so it the implanted Biosheet may rupture before the Biosheet becomes thicker after implantation. However, since the Biosheet can form a thick sheet of about 3 mm by adjusting the gap distance between the center bar and outer cage of the mold [16], it was thought that the Biosheet’s thickness could be increased to the actual strength corresponding to the human diaphragm.

Despite the thickness change in the Biosheet after implantation, the spring coefficient of the toe region was maintained at a value equivalent to that of the native diaphragm. This was realized by decreasing Young's modulus of the toe region. Furthermore, the transition strain of the Biosheet after implantation also changed to the

value equivalent to that of the native tissue. Furthermore, the maximum spring constant has changed to the value equivalent to that of native tissue, which seems to have been realized by increasing the sheet thickness. This means that the elasticity is equivalent to that of the native tissue over the entire extension area. This may be a major advantage of Biosheets over other artificial materials such as conventional ePTFE sheets. The abdominal hernia recurrence rate is reported to be attributed to the characteristic difference in the elastic modulus [21]. A lightweight mesh has been used in order to suppress the fiberizing reaction, but it seems to be effective in reducing the recurrence rate [22]. The elasticity is evaluated with a load for a certain elongation value [23]. However, the curve of the polymer used for these artificial materials is not a J-curve but a convex one [24], and the elasticity corresponding to the low strain range is greatly different from that of the biological tissue showing the J-curve. Therefore, the reaction force characteristics against elongation actually differ in practice. Since the overall reaction force characteristics of the Biosheet after implantation are approximated almost from the low strain region to the high region, there is a possibility of reducing the recurrence rate, which is a future research topic.

I expected material parameters such as the ultimate tensile strength and Young's modulus of Biosheets after implantation will to be adapted to values equivalent to native tissue, but it was not realized in 3 months. However, since actual strength and actual elasticity are realized by changing the thickness, the mechanical function is considered to be sufficient for the living body. Another future subject is to monitor long-term change in the material parameters.

3.1.5 Conclusion

I evaluated the availability of Biosheet implantation to the diaphragm of beagle dogs. The implanted Biosheet properties changed to match those of the Beagle diaphragm one month after implantation: the actual strength and the real elasticity were therefore considered to have changed to values corresponding to the beagle diaphragm, by changing the Biosheet thickness. The adaptation of live living actual elasticity may reduce the hernia recurrence rate and will be investigated further in the future.

3.1.6 Refences

[1] Losty PD. Congenital diaphragmatic hernia: where and what is the evidence? Semin Pediatr Surg 2014;23(5):278–82.

[2] Said SM, Moir CR, Ishitani MB, et al. Successful thoracoscopic staged repair of bilateral congenital diaphragmatic hernia. J Pediatr Surg 2010;45(4):5–8.

[3] Kitano Y, Lally KP, Lally PA. Late-presenting congenital diaphragmatic hernia. Journal of Pediatric Surgery, vol. 40, no. 12, pp. 1839–1843, 2005.

[4] Gaur P, Chawla A, Verma K, Mukherjee S, Lalvani S, Malhotra R, Mayer C. Characterisation of human diaphragm at high strain rate loading. J Mech Behav Biomed Mater. 2016; 60: 603-616

[5] Champion JK, Rock D :Laparoscopic mesh cruroplasty for large paraesophageal hernias. Surg Endsc 2003;17:551 – 553

[6] Garriboli M, Bishay M, Kiely EM, Drake DP, Curry JI, Cross KM, Eaton S, De Coppi P, Pierro A. Recurrence rate of Morgagni diaphragmatic hernia following laparoscopic repair. Pediatr Surg Int. 2013; 29: 185-189.

[7] Frantzides CT, Madan AK, Carlson MA, Stavropoulos GP. A prospective, randomized trial of laparoscopic polytetrafluoroethylene (PTFE) patch repair vs simple cruroplasty for large hiatal hernia. Arch Surg. 2002 Jun;137(6):649-52.

[8] Wadhwa A, Surendra JB, Sharma A, Khullar R, Soni V, Baijal M, Chowbey PK. Laparoscopic repair of diaphragmatic hernias: experience of six cases. Asian J Surg. 2005; 28: 145-150.

[9] Grethel EJ, Cortes RA, Wagner AJ, Clifton MS, Lee H, Farmer DL, Harrison MR, Keller RL, Nobuhara KK. Prosthetic patches for congenital diaphragmatic hernia repair: Surgisis vs Gore-Tex. J Pediatr Surg. 2006; 41: 29-33

[10] Riehle KJ, Magnuson DK, Waldhausen JH. Low recurrence rate after Gore-Tex/Marlex composite patch repair for posterolateral congenital diaphragmatic hernia. J Pediatr Surg. 2007; 42: 1841-1844.

[11] K.P. Lally, H.W. Cheu, W.D. Vazquez, Prosthetic diaphragm reconstruction in the growing animal. J Pediatr Surg, 1993; 28: 45-47

[12] Gonzalez R, Hill SJ, Mattar SG, Lin E, Ramshaw BJ, Smith CD, Wulkan ML. Absorbable versus nonabsorbable mesh repair of congenital diaphragmatic hernias in a growing animal model. J Laparoendosc Adv Surg Tech A. 2011; 21: 449-454.

[13] Zhang XY, Yanagi Y, Sheng Z, Nagata K, Nakayama K, Taguchi T. Regeneration of diaphragm with bio-3D cellular patch. Biomaterials. 2018; 167: 1-14.

[14] Novosel EC, Kleinhans C, Kluger PJ. Vascularization is the key challenge in tissue engineering. Adv Drug Deliv. 2011;63:300–11.

[15] Furukoshi M, Moriwaki T, Nakayama Y. Development of an in vivo tissue-engineered vascular graft with designed wall thickness (biotube type C) based on a novel caged mold. J Artif Organs. 2016;19:54–61.

[16] Terazawa T, Nishimura T, Mitani T, Ichii O, Ikeda T, Kosenda K, Tatsumi E, Nakayama Y, Wall thickness control in biotubes prepared using type-C mold. J Artif Organs. 2018; 21: 387-391.

[17] Nakayama Y, Furukoshi M, Feasibility of in-body tissue architecture in pediatric cardiovascular surgery: development of regenerative autologous tissues with growth potential. J. Pediatr. Cardiol. Cardiovasc. Surg. 2018; 2 : 28-36

[18] Elliott, D.M., Setton, L.A. Anisotropic and inhomogeneous tensile behaviour of the human annulus fibrosis: experimental measurement and material model predictions. J. Biomech. Eng. 2001; 123: 256–263.

[19] Lynch, H.A., Johannessen, W., Wu, J.P., Jawa, A., Elliott, D.M. Effect of fiber orientation and strain rate on the nonlinear uniaxial tensile material properties of tendon. J. Biomech. Eng. 2003; 125: 726–731.

[20] Duprey A, Khanafer K, Schlicht M, Avril S, Williams D, Berguer R. In vitro characterisation of physiological and maximum elastic modulus of ascending thoracic aortic aneurysms using uniaxial tensile testing. Eur J Vasc Endovasc Surg 2010; 39: 700-707.

[21] DuBay DA, Wang X, Adamson B, Kuzon WM, Dennis RG, Franz MG. Mesh incisional herniorrhaphy increases abdominal wall elastic properties: a mechanism for decreased hernia recurrences in comparison with suture repair. Surgery. 2006;140:14–24.

[22] CN Brown and JG Finch. Which mesh for hernia repair? Ann R Coll Surg Engl. 2010; 92: 272–278.

[23] Klosterhalfen B, Junge K, Klinge U. The lightweight and large porous mesh concept for hernia repair. Expert Rev Med Devices 2005; 2: 103–17.

[24] Nunes LCS, Dias FWR, da Costa Mattos HS (2011) Mechanical behavior of polytetrafluoroethylene in tensile loading under different strain rates, Polymer Testing 30:791-796

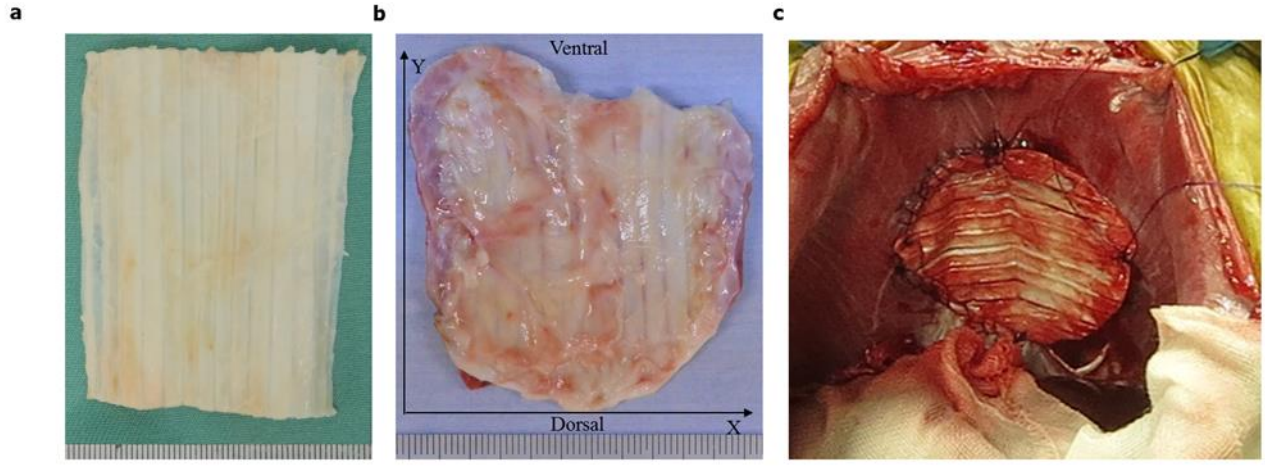

Figure 3-1-1. (a) Pre-implant Biosheet formed with mold. (b) Sewing of Biosheet to defect in beagle diaphragm. (c) Biosheet harvested three months after implantation. The Y direction indicates the ventral-dorsal direction, and the X direction indicates the direction orthogonal to the Y direction.

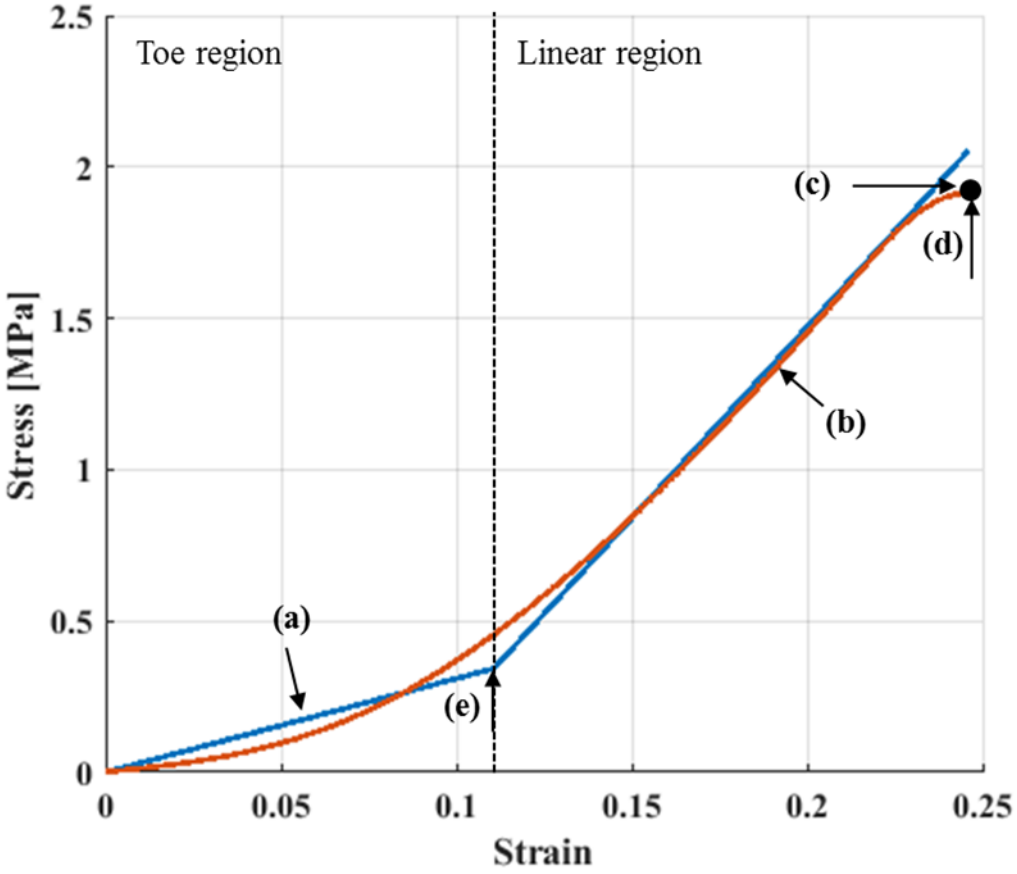

Figure 3-1-2. Stress–strain curve obtained by performing the uniaxial tensile test of Biosheets. Bilinear fitting lines are also drawn. (a) Transition strain, which is the strain value at the position where the fitting line intersects. The strain region lower than the "transition strain" is the "toe region" and the higher strain region is the "linear region". (b) Young's modulus (toe region), which is the slope of the toe region approximated by bilinear fitting. (c) Maximum Young's modulus, which is the maximum slope value in the stress–strain curve. (d) Ultimate tensile strength, which is the maximum stress value in the stress–strain curve. (e) Fracture strain, which is the strain value at break in the stress–strain curve.

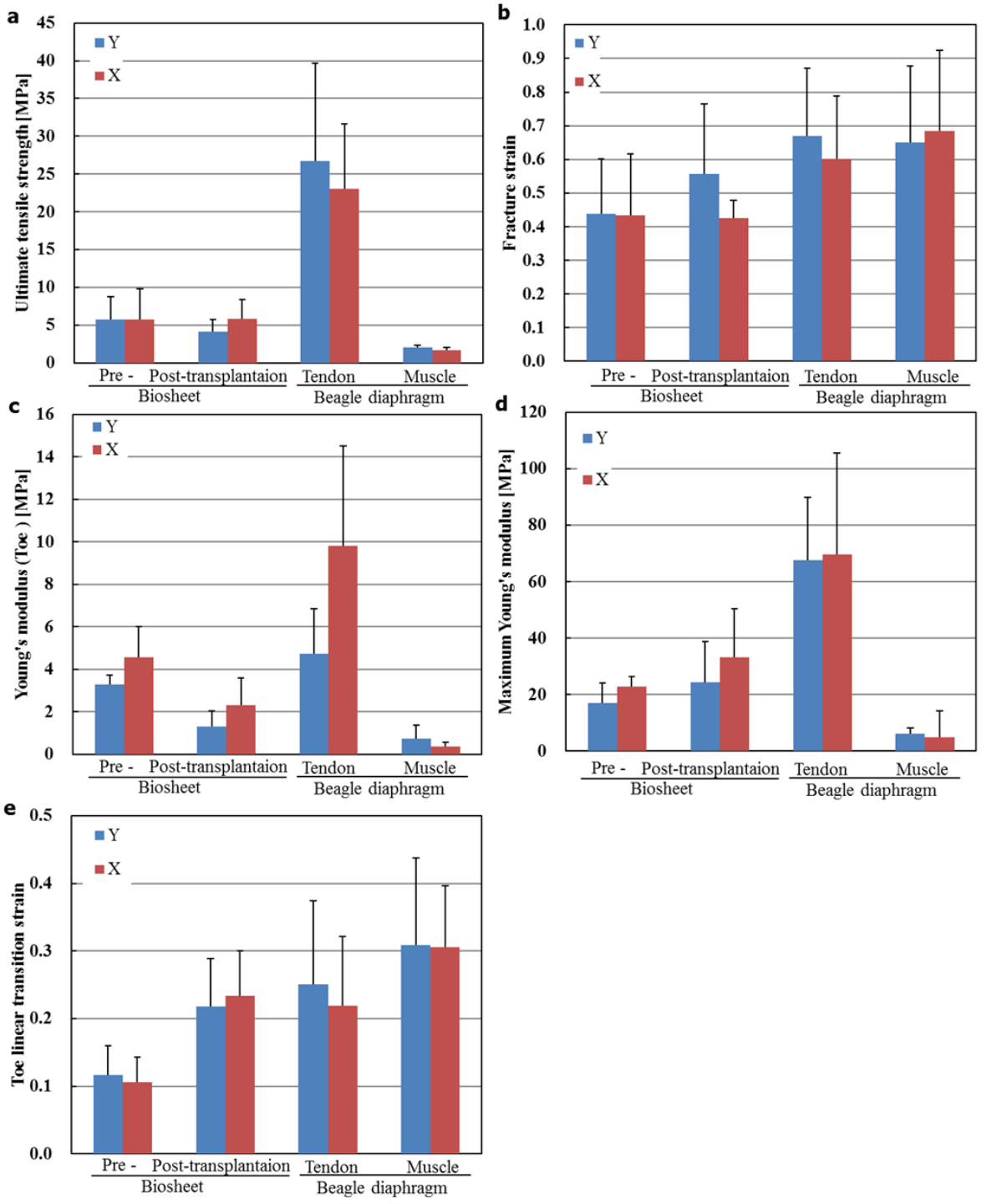

Figure 3-1-3. Anisotropy of the mechanical property values for each tissue.

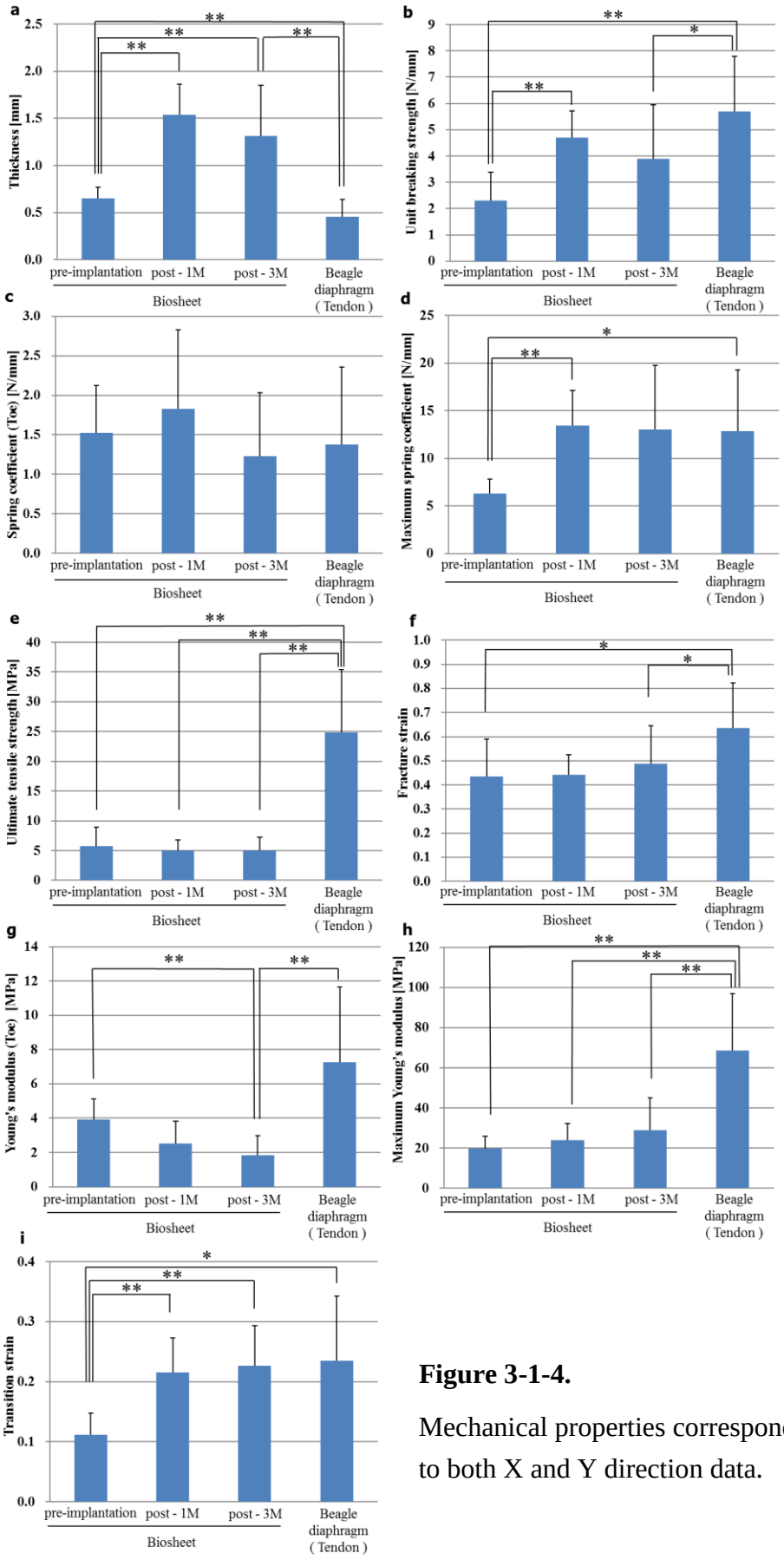

Figure 3-1-4.

Mechanical properties corresponding to both X and Y direction data.

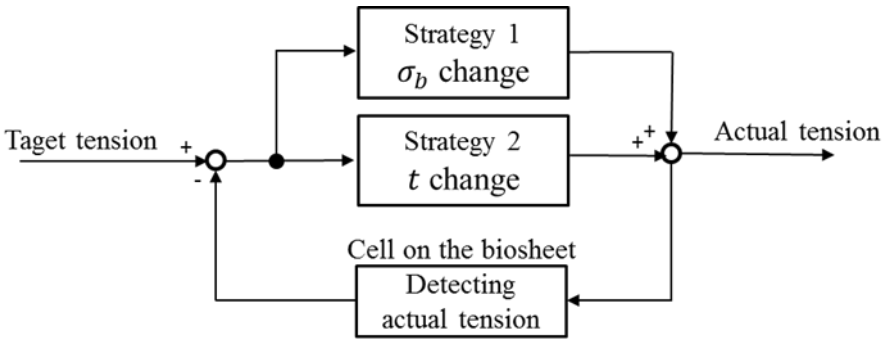

Figure 3-1-5. Control block model diagram of diaphragm tension adjustment mechanism.

Chapter 3.2

Chronic phase evaluation of Biosheet after implantation to beagle abdominal wall

3.2.1 Introduction

Synthetic implants, such as a Polypropylene mesh [1] or an expanded polytetrafluoroethylene sheet [2], have been widely used for the treatment of large abdominal wall hernias during reconstruction and reinforcement. They have sufficient tensile strength to support the abdominal viscera, but have been reported to cause fibrotic inclusion, infection, erosion, and mesh extrusion. However, tissue-based biomaterials have been used owing to their biocompatibility. As the biomaterials, human dermis (Alloderm®) [4], porcine dermis (Permacol™, Strattice®), and porcine small-intestinal submucosa (Surgisis™) [5] are also commercially available. However, the problem of low repair strength is reported as compared with the case of using self-organization. As the healing and reabsorption of the biological skeleton occurs, loss of tissue support over time may result in relaxation or bulging of the abdominal wall and hernia recurrence. Moreover, for pediatric surgery, there is an urgent need to develop large patches that can grow with the individual [6], and for patches made without foreign material.

Nakayama et al. have developed autologous prosthetic tissues using in-body tissue

architecture (iBTA) [7]. iBTA is a cell-free tissue engineering technology that can produce implantable tissues with the desired shape and appropriate mechanical properties via simple subcutaneous embedding of a specially designed mold. The tissues developed using the iBTA technique include sheet-like tissues called Biosheets. In our previous study, Biosheets were successfully implanted as allogeneic substitutes in the corneal stroma in a rabbit model with biological stability and biocompatibility. Biosheet is the first corneal material based on the novel concept of conversion to transparency in situ [8]. Biosheets have been applied to an aortic valve leaflet material for aortic valve neo-cuspidization (Ozaki method) [9]. Biosheet also functioned with tissue regeneration as an aortic valve for 3 months [10]. Therefore, it was shown that Biosheet had both mechanical strength and regenerative ability. Recently, Nakayama et al. reported that bovine Biosheets could be useful as off-the-shelf materials, where the Biosheets functioned as an abdominal wall repair material even in xeno-implantation in mid-term histological observation [11]. However, there are no reports in long-term implantation studies using Biosheets, particularly with respect to mechanical changes.

In this pilot study, I aimed to investigate whether Biosheets possess tissue regeneration ability as a restorative material while maintaining mechanical function for a long time. Therefore, a large area of abdominal wall defect, clinically requiring prosthetic treatment, was prepared in a beagle dog model and patch implantation with Biosheets was performed.

3.2.2 Materials and Methods

3.2.2.1 Ethical Approval

All animal experiments were performed in accordance with the Guide for the Care

and Use of Laboratory Animals, published by the United States National Institutes of Health (NIH Publication No. 85-23, received 1996). The animal experiments were approved.

3.2.2.2 Preparation of Biosheets

The cylindrical rods (n = 4, diameter 20 mm, length 5 cm, Tigers Polymer, Osaka, Japan) used as the mold for Biosheet preparation. Pre-anesthetic medication included 5 mg/kg ketamine, 0.02 mg/kg IV buprenorphine, and 0.025 mg/kg IM atropine sulfate, and anesthesia was induced by 15 mg/kg IV pentobarbital and maintained by bolus induction of a pentobarbital IV at a quarter or half of the initial dose. The mold was embedded into subcutaneous pouches of female beagle dogs (weight ca. 10 kg). The dogs were raised in the cage at the animal management department of National Cerebral and Cardiovascular Center maintained at a temperature of 20-28°C, humidity of 40-60%, and light period from 7 am to 19 pm. After 2 months of regular rearing, the molds were harvested with the surrounding connective tissues. The tubular tissues formed around the molds were extracted. Biosheets (size 5 cm × 5 cm, thickness ca. 0.5 mm) were obtained by longitudinally cutting the tubular tissues. The Biosheets were stored in 70% ethanol prior to implantation.

3.2.2.3 Implantation of Biosheets

The abdomen, from the xiphoid process to the groin, was surgically prepped. A 10 cm midline abdominal incision was made from approximately 2 cm below the xiphoid process to the pubic symphysis. Bilateral skin flaps were raised using blunt dissection of the subcutaneous layer. Two standardized 5 cm × 5 cm incisional defects were made at

the midline, identified by the linea alba, by excising a full thickness portion of the abdominal wall, including the peritoneum, abdominal wall muscle, and fascia. After soaking in a saline solution for a minimum of 10 min prior to use, Biosheets were held in position with simple interrupted sutures in the corner, followed by a running suture (3-0 PROLENE, Ethicon) surrounding the perimeter of the implant, attaching the dermis as an overlay to the abdominal wall musculature. Subcutaneous tissues were closed using multi-layer suturing with polydioxanone sutures (3-0 PDS, Ethicon) and the skin was then closed using simple nylon sutures (3-0 nylon, ELP). The dogs were raised in the cage at the animal management room of National Cerebral and Cardiovascular Center maintained at a temperature of 20-28°C, humidity of 40-60%, and light period from 7 am to 19 pm. At one year post-implementation, dogs were humanely euthanized with a barbiturate (75 mg/kg IV). Following euthanasia, lateral skin incisions were made to expose the surgical site without disruption. Evidence of bowel adhesion, hernia formation, or abdominal bulging was macroscopically observed. No control was used in this study.

3.2.2.4 Histological Examination

Samples were fixed with 10% neutral buffered formalin, embedded in paraffin, and sectioned into 3–5 μm sections. The specimens were stained with Masson's trichrome stain for collagen (blue) and muscle (red).

3.2.2.5 Measurement of Mechanical Properties

Biosheets pre- (n = 5) and post-implantation (n = 4) and native abdominal walls (n = 2) were immersed in a saline solution and cut into a dumbbell shape (tensile area: 5

mm × 5 mm) as samples. Biosheet thickness was measured using optical coherence tomography (OCT, IVS-2000, Santec, Aichi, Japan) [3]. Tissue strength was measured using a uniaxial tensile tester (EZ-LX, Shimadzu, Kyoto, Japan) in air immediately after picking up from saline. The dumbbell-shaped sample was placed between two chucks. The initial length of the samples was set using a preliminary load of 0.02 N. The stress was loaded to braking at a rate of 0.5 mm/sec. The breaking strength was defined as the maximum load value (N) at the highest point of the obtained load-extension curve. The unit breaking strength was defined as the value obtained by dividing the breaking strength by the sample width. The spring coefficient of the 0-40% region was defined as the slope calculated by the linear least squares for the 0 to 40% strain range data of the load-extension curve. The maximum spring coefficient was defined as the maximum slope of the curve. True stress / true strain were calculated as previously reported [12]. The ultimate tensile strength was determined based on the maximum value of stress and the maximum Young's modulus (MPa) was determined from the maximum slope of the stress-strain curve. The Young's modulus of the 0-40% strain region was calculated as the slope using the linear least squares method of the strain-strain curve of the 0-40% region.

3.2.2.6 Statistical analysis

The results were expressed as mean ± standard deviation. Analysis of variance and t test were used to determine significant differences between the groups and $p < 0.05$ was considered significant.

3.2.3 Results

Two beagles underwent patch implantation of Biosheets in surgical defects in their abdominal wall. The abdominal skin was dissected (Figure 3-2-1a), and defects of all layers of 5 cm square were prepared on the abdominal wall (Figure 3-2-1b). Suturing of the Biosheet and the abdominal wall was easy (Figure 3-2-1c) and damage, such as cutting, did not occur on the Biosheets. All patch procedures were completed without any complications such as anastomotic leak (Figure 3-2-1d). All animals resumed normal appetite, urination, and defecation patterns within 24 hours post-operation. No abnormal abdominal wall defects or hernia formation, abdominal bulging, or infection occurred during the observation period (Figure 3-2-1e).

One year post-implantation, the white abdominal membrane was completely covered on the implanted Biosheet area under abdominal skin (Figure 3-2-1f). Adhesion of bowel tissue on the peritoneal cavity side was minor (Figure 3-2-1g) and could be easily detached where formation of a wrinkle-like peritoneum was macroscopically observed (Figure 3-2-1h). Little seromas or shrinkage of the materials was noticed. In the histological examination, the linea alba layer was formed (Figure 3-2-2a). The rectus abdominis muscle was observed in the newly formed collagen layer made of collagen type I (Figure 3-2-2b) and the peritoneum was formed entirely on the peritoneal cavity surface (Figure 3-2-2c), resulting in the partial regeneration of the three-layered abdominal wall.

The thickness of the Biosheet-implanted portion was approximately 2.5 mm, which was approximately 5-fold greater than that of the Biosheet pre-implantation and approximately 70% that of the native abdominal wall (Figure 3-2-3a). The unit breaking strength and the spring coefficient of the Biosheet-implanted portion increased

significantly with thickness and both were much higher than that of the native tissue (Figure 3-2-3b, c). However, the spring coefficient in the low strain region of up to 40% was significantly reduced to approximately 10% post-implantation, similar to the native tissue value (Figure 3-2-3d).

Ultimate tensile strength was significantly higher than pre-implantation and was approximately 6-fold higher than the native tissue value (Figure 3-2-3e). The fracture strain was also significantly greater than pre-implantation, similar to the native tissue (Figure 3-2-3f). Although the maximum Young's modulus pre- and post-implantation was approximately 6-fold higher than that of the native tissue (Figure 3-2-3g), in the low strain region of up to 40% the Young's modulus was significantly reduced to approximately 16% post-implantation, close to the native tissue value (Figure 3-2-3h).

3.2.4 Discussion

Our study showed that the allogenic Biosheet can be used for repairing relatively large abdominal wall defects with no herniation and appears to regenerate muscular tissue one year post-implantation. Moreover, no abnormal events, such as chronic inflammation, were observed. Therefore, the long-term reliability of the allogenic Biosheet was demonstrated for the first time. One year post-implantation, the original tissue of the Biosheet disappeared and its tissue was almost completely replaced by the host's own tissue, consisting of the linea alba and the peritoneum, and the rectus abdominal muscle between them. The three-layered abdominal wall structure was recognized with little distortion in both the Biosheet implantation cases. Therefore, at least partial abdominal wall reconstruction was induced by the allogenic Biosheet patching. In our recent report, iBTA-induced tubular tissues, named Biotubes, could be

expanded and elongated with an increase in the recipient body weight from ca. 3 kg to ca. 10 kg in 1 year, which is the first evidence about the growth ability of the iBTA tissues [7]. However, almost all prosthetic patches can be associated with infection, allergic reaction, recurrence, and thoracic deformity owing to their increasingly disproportionate size as the children grow [13]. It is considered that Biosheet, which is one of the iBTA tissues, also has growth ability. Therefore, Biosheet may be useful for hernia treatment in growing children. However, owing to limited number of animals used, this study is only suggestive, but provides valuable insights to the field of regenerative medicine. In order to test the reliability of the results obtained in this study, additional implant studies with detailed histological examinations are required in addition to further long-term implant studies.

Tissue engineering is an emerging strategy for repairing damaged tissues or organs. It has been suggested that the combination of biomaterial scaffolds with stem cells can accelerate tissue regeneration and result in tissue repair with natural structural and functional properties [14-16]. Decellularized ECM scaffolds have the potential of regenerating the structure and function of their native tissue over commercially available matrices from other tissues [17,18]. Those decellularized ECM scaffolds have been used in combination with stem cells to construct composite tissues that have been utilized successfully in tissue repair, including diaphragmatic repair. In contrast, Bio-3D printing has been developed to create these tissues [19,20]. Cells on 3D culture can better reflect in vivo physiological conditions than cells cultured in two dimensions. This method, which uses a temporary immobilization support structure to produce tissues that only consist cells without a foreign material, positions various cells in an arbitrary 3D space. Upon transplantation of cellular patches into rats with surgically

created diaphragmatic defects, histology analysis results revealed regeneration of muscle structure, neovascularization, and neuronal networks within the reconstructed diaphragms [21].

In clinical practice, the formation of autologous Biosheets in a patient's body is unsuitable for emergency surgery. In addition, the procedure for subcutaneous embedding and extracting the mold is invasive. Therefore, I think that it is necessary to investigate the possibility of using animal-derived sheets as an abdominal wall restorative material. Recently, a Biosheet subcutaneously prepared in a cow was applied to repair the abdominal wall defect of a dog [11]. Decomposition was nearly complete after 3 months and the Biosheet was replaced by autologous collagenous connective tissue without rejection. After 5 months, the abdominal wall muscle elongated from the periphery of the newly formed collagen layer and the peritoneum was formed on the peritoneal cavity surface. Therefore, bovine Biosheets can be useful as off-the-shelf materials for abdominal wall repair.

Polypropylene, polyester, polyglactin, and ePTFE mesh have been used as hernia repair materials; the strength required for the mesh is estimated to be 3.2 N/mm [22]. Therefore, a Biosheet with 4.4 N/mm breaking strength should have sufficient strength. One year post Biosheet implantation, the implanted area became thick, resulting in significant high actual strength and maximum elasticity. However, the spring coefficient of the implanted area in the low strain region of the practical range was close to the native value. In addition, although there was little difference in the maximum Young’s modulus pre- and post-implantation, the Young's modulus in the low strain region of the practical range was close to the native value. Taken together, these results indicate that Biosheet implantation led to adaptation in the practical range of the mechanical

properties.

Collagen, the main Biosheet component, has a stress-strain curve known as the J-curve and has a toe linear and failure region [23]. The toe region occurs where collagen fibers gradually transition from a relaxed state to a tensioned state. Expansion of this toe region was observed post-implantation, which is thought to correspond to an increase in the amount of collagen relaxation. Unlike the properties of artificial materials, such as ePTFE [24], the Biosheet has J-curve characteristics, providing the advantage that it can conform to the native characteristics throughout the practical strain region.

3.2.5 Conclusion

To our knowledge, this pilot study was the first to report on long-term implantation of Biosheets (for a year) and demonstrated that Biosheets could repair large abdominal wall defects without any complications in two beagle dogs. The partial regeneration of abdominal wall was observed in both cases. The results indicated that Biosheets serve as a reliable abdominal wall restorative material. This study provides valuable insights to the field of regenerative medicine. However, to test the reliability of the results obtained in this study, another implantation study with detailed histological examination is currently being conducted in addition to further long-term implantation studies.

3.2.6 References

[1] Pandey H, Thakur DS, Somashekar U, Kothari R, Agarwal P, Sharma D (2018) Use of polypropylene mesh in contaminated and dirty strangulated hernias: short-term results. Hernia [Epub ahead of print]

[2] Stirler VMA, de Haas RJ, Raymakers JTFJ, Rakic S (2018) Persistent posterior seroma after laparoscopic repair of ventral abdominal wall hernias with expanded polytetrafluoroethylene mesh: prevalence, independent predictors and detached tacks : Retrospective review. Hernia 22:285–291

[3] Bryan N, Ahswin H, Smart N, Bayon Y, Wohlert S, Hunt JA (2014) The in vivo evaluation of tissue-based biomaterials in a rat full-thickness abdominal wall defect model. J Biomed Mater Res B Appl Biomater 102:709–20

[4] Filisetti C, Costanzo S, Marinoni F, Vella C, Klercy C, Riccipetitoni G. Effectiveness and properties of the biological prosthesis Permacol™ in pediatric surgery: A large single center experience. (2016) Ann Med Surg (Lond) 7:48-54.

[5] Eastwood MP, Daamen WF, Joyeux L, Pranpanus S, Rynkevic R, Hympanova L, Pot MW, Hof DJ, Gayan-Ramirez G, van Kuppevelt TH, Verbeken E, Deprest J (2018) Providing direction improves function: Comparison of a radial pore-orientated acellular collagen scaffold to clinical alternatives in a surgically induced rabbit diaphragmatic tissue defect model. J Tissue Eng Regen Med [Epub ahead of print]

[6] Nagata K, Usui N, Terui K, Takayasu H, Goishi K, Hayakawa M, Tazuke Y, Yokoi A, Okuyama H, Taguchi T (2014) Risk factors for the recurrence of the congenital diaphragmatic hernia—report from the long-term follow-up study of Japanese CDH study group. Eur J Pediatr Surg 25:9–14

[7] Nakayama Y, Furukoshi M (2018) Feasibility of in-body tissue architecture in pediatric cardiovascular surgery: development of regenerative autologous tissues with growth potential. J Pediatr Cardiol Cardiac Surg 2:28–36

[8] Takiyama N, Mizuno T, Iwai R, Uechi M, Nakayama Y. In-body tissue-engineered collagenous connective tissue membranes (BIOSHEETs) for potential corneal stromal substitution (2016) J Tissue Eng Regen Med 10:E518–E526

[9] Ozaki S, Kawase I, Yamashita H, Uchida S, Takatoh M, Kiyohara N (2018). Midterm outcomes after aortic valve neocuspidization with glutaraldehyde-treated autologous pericardium. J Thorac Cardiovasc Surg 155:2379–2387

[10] Okamoto K, Kawashima T, Nakayama Y, Anai H, Wada T, Takebayashi S, Shuto T, Kozaki S, Miyamoto S (2018). Aortic Valve Reconstruction Using In-body Tissue-Engineered Collagenous Connective Tissue Membranes,BIOSHEETs, in a 3-month Goat Model. Circulation 134:A13472

[11] Nakayama Y, Oshima N, Tatsumi, Ichii O, Nishimura T (2018) iBTA-induced bovine Biosheet for repair of abdominal wall defects in a beagle model: proof of concept. Hernia in press

[12] Duprey A, Khanafer K, Schlicht M, Avril S, Williams D, Berguer R (2010) In vitro characterisation of physiological and maximum elastic modulus of ascending thoracic aortic aneurysms using uniaxial tensile testing. Eur J Vasc Endovasc Surg 39: 700-707

[13] Clark RH, Hardin WD Jr, Hirschl RB, Jaksic T, Lally KP, Langham MR Jr, Wilson JM (1998) Current surgical management of congenital diaphragmatic hernia: a report from the congenital diaphragmatic hernia study group. J Pediatr Surg 33:1004–1009

[14] Pashneh-Tala S, MacNeil S, Claeyssens F (2016) The Tissue-Engineered Vascular Graft-Past, Present, and Future. Tissue Eng Part B Rev 22:68-100

[15] Shoji T, Shinoka T (2018) Tissue engineered vascular grafts for pediatric cardiac surgery. Transl Pediatr 7:188-195

[16] Klinger A, Kawata M, Villalobos M, Jones RB, Pike S, Wu N, Chang S, Zhang P, DiMuzio P, Vernengo J, Benvenuto P, Goldfarb RD, Hunter K, Liu Y, Carpenter JP, Tulenko TN (2016) Living scaffolds: surgical repair using scaffolds seeded with human adipose-derived stem cells. Hernia 20:161-70

[17] Ghetti M, Papa V, Deluca G, Purpura V, Ruscelli P, Melandri D, Capirossi D, Nigrisoli E, Minghetti P, Bondioli E, Cenacchi G (2018) Histological and ultrastructural evaluation of human decellularized matrix as a hernia repair device. Ultrastruct Pathol 42:32-38

[18] Fernandez-Moure JS, Van Eps JL, Rhudy JR, Cabrera FJ, Acharya GS, Tasciotti E, Sakamoto J, Nichols JE (2016) Porcine acellular lung matrix for wound healing and abdominal wall reconstruction: A pilot study. J Tissue Eng 7:2041731415626018

[19] Moldovan NI, Hibino N, Nakayama K (2017) Principles of the Kenzan Method for Robotic Cell Spheroid-Based Three-Dimensional Bioprinting. Tissue Eng Part B Rev 23:237-244

[20] Maiullari F, Costantini M, Milan M, Pace V, Chirivì M, Maiullari S, Rainer A, Baci D, Marei HE, Seliktar D, Gargioli C, Bearzi C, Rizzi R (2018) A multi-cellular 3D bioprinting approach for vascularized heart tissue engineering based on HUVECs and iPSC-derived cardiomyocytes 8:13532

[21] Zhang XY, Yanagi Y, Sheng Z, Nagata K, Nakayama K, Taguchi T (2018) Regeneration of diaphragm with bio-3D cellular patch. Biomaterials 167:1-14

[22] Brown CN, Finch JG (2010) Which mesh for hernia repair? Am R Coll Surg Engl 92:272-278

[23] Roeder BA, Kokini K, Sturgis JE, Robinson JP, Voytik-Harbin SL (2002) Tensile mechanical properties of three-dimensional type I collagen extracellular matrices with varied microstructure. J Biomech Eng 124 :214-222

[24] Nunes LCS, Dias FWR, da Costa Mattos HS (2011) Mechanical behavior of polytetrafluoroethylene in tensile loading under different strain rates, Polymer Testing 30:791-796

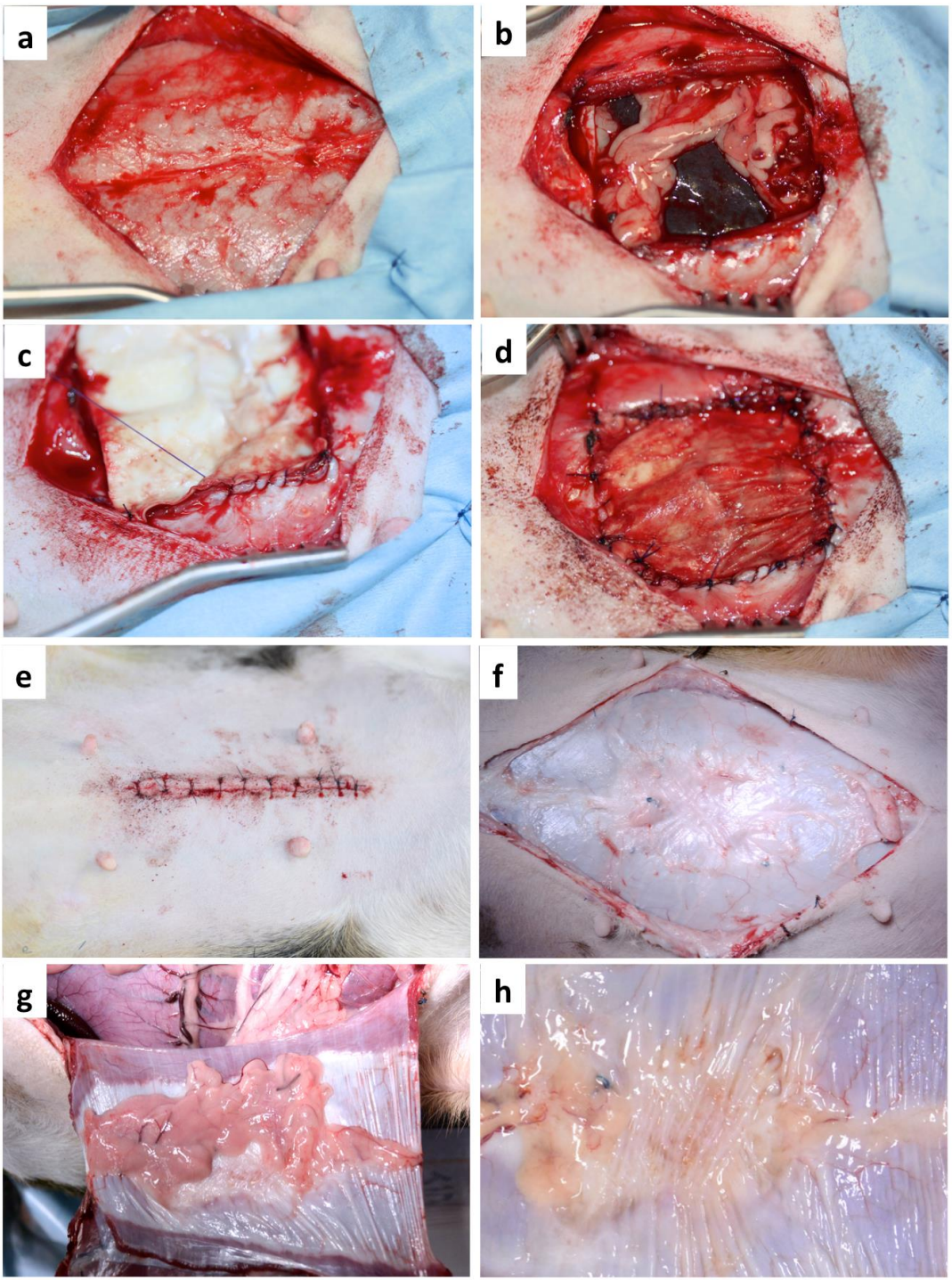

Figure 3-2-1. Photos of the dissected abdominal skin of a beagle dog (a) and the defect of all layer of its peritoneal (b). Suturing of the Biosheet and the peritoneal (c,d). The abdominal wound closed with nylon sutures (e). The peritoneal at one year post-implantation (f). The peritoneal cavity surface with bowel tissue adhesion (g) and after its detachment (h).

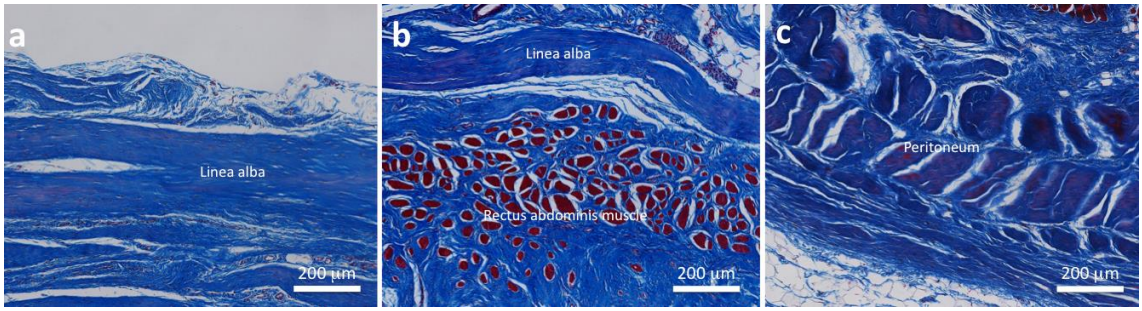

Figure 3-2-2. Histological cross-sectional micrographs of the beagle abdominal wall at the abdominal skin side (a), the mid portion (b), and the peritoneal cavity side (c) after one-year implantation of the Biosheets stained with Masson's trichrome stain.

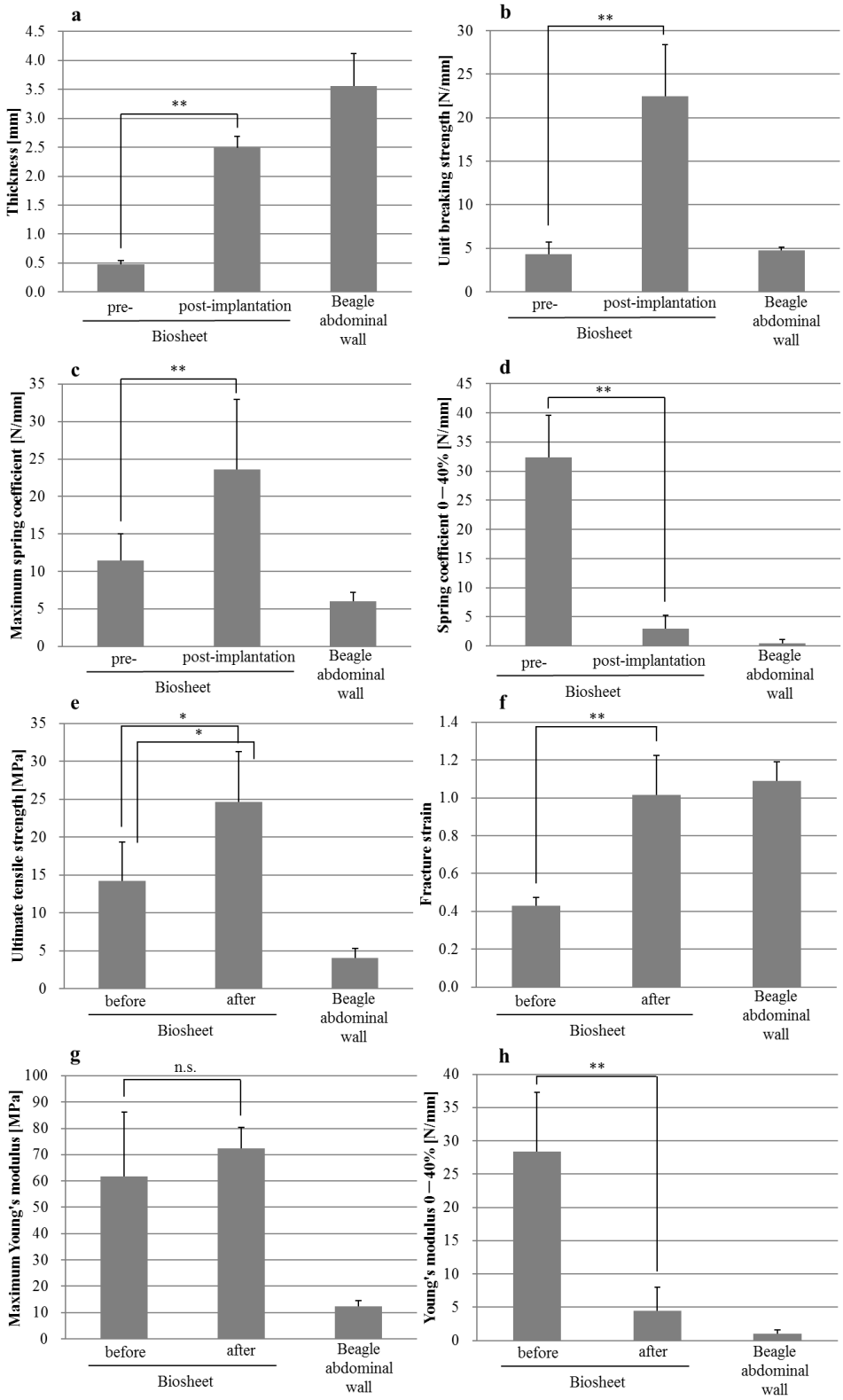

Figure 3-2-3. Physical properties of Biosheets before and after implantation. The significance levels by statistical analysis are * $p < 0.05$ and ** $p < 0.01$.

Chapter 4

Conclusion

This thesis comprises studies on the mechanical analyses of in-body tissue formation and in-situ adaptation processes in regenerative medicine based on in-body tissue architecture, which had been carried out from 2016 to 2019 at the Department of Artificial Organs, or the Department of Regenerative Medicine and Tissue Engineering of National Cardiovascular Center Research Institute.

Chapter 2-1.

Collagenous tubular tissues Biotubes, formed by in-body tissue engineering, were implanted already as clinical vascular grafts in hemodialysis surgery. In almost all previous studies, Biotubes were stored in 70% alcohol before implantation, but the influence of alcohol concentration on the mechanical properties of Biotubes had not been investigated in depth.

The mechanical properties of Biotubes, stored at room temperature in two different concentrations of ethanol (10% or 70%), were compared through fatigue and tensile tests. Biotubes with an internal diameter of 6 mm and wall thickness of ca. 2 mm were prepared by subcutaneous embedding of molds into goats for 2 months, and stored in 10% or 70% ethanol for 20 days. In the fatigue test by repeatable loading of tension corresponding to arterial pressure, Biotubes stored in 10% ethanol elongated by

approximately 80% in length, but in 70% solution, the elongation was less than 20%. sStoring Biotubes in high concentration ethanol prevented stretching under maintenance of compliance.

Chapter 2-2.

Biotubes with large diameter were prepared with controlling of their wall thickness. Four types of molds with different gap distances for tissue formation were prepared and surgically embedded in the abdominal subcutaneous pouches of Holstein cows. The wall thickness of the Biotubes obtained was approximately 1–3 mm, which corresponded to approximately 80% of each gap distance. Their breaking strength almost linearly increased with the wall thickness of the Biotubes. The strength of the Biotubes having wall thickness of about 1.5 mm or more was higher than those of beagle blood vessels. The thickest Biotubes were as strong as bovine pericardium and may be used as an alternative trachea graft.

Chapter 2-3.

Cylindrical molds with line slits arranged in an alternating or parallel pattern were subcutaneously embedded in goats for several months. The tubular tissues formed in the molds were dried and then cut in the longitudinal direction, thus forming the sheet-like Biosheets. Thickness mapping of the Biosheets showed that their entire surface, except for the line-projection portions, was smooth without any defects. The average wall thickness could be controlled over a range of ca. 0.2–0.5 mm by changing the size of the gap (0.75–1.5 mm) in the molds. The alternating slit-patterned Biosheets were found to be almost isotropic in their mechanical properties (ultimate tensile

strength, fracture strain, and Young's modulus). Although the composition of the Biosheet wall was heterogeneous in terms of its density (which varied with the thickness), the breaking strength of all the alternating-patterned Biosheets increased almost linearly with the thickness within the range of the thickness of glutaraldehyde-treated human pericardium, and was larger than that of human aortic valve leaflets. Therefore, the alternating-patterned Biosheets can be used as an alternative aortic leaflet material in AVNeo.

Chapter 3-1.

The in-situ mechanical adaptation of tissue-engineered collagenous sheets (Biosheets) was evaluated in the repair process of diaphragmatic defects.

After rinsing with physiological saline, Biosheets were implanted to elliptical defects of beagle diaphragm. Mechanical properties before and after 1 or 3 months of implantation were measured via a uniaxial tensile test.

There were no complications in any observation period. Slight anisotropy of mechanical properties was observed in the Biosheets before and after implantation. At 1 month of implantation, the actual strength and elasticity of the Biosheet-implanted parts became equivalent to those of the beagle tissues when the wall thickness of the implants were about three times that of beagle diaphragm tissues, with little change in the Biosheet material properties (tensile strength, fracture strain, and Young's modulus) after implantation. Dimensional, mechanical, and material properties of the Biosheet-implanted parts remained unchanged at 3 months of implantation. By increasing Biosheet thickness without changing material properties within 1 month, the Biosheets acquired the bulk strength similar to that of the native diaphragm tissues, thus

preventing collapse. Biosheets even with thin thickness may be useful as a diaphragmatic repair material.

Chapter 3-2.

Biosheets were implanted to replace same-size defects in the abdominal wall of two beagles in an allogenic manner. The Biosheets were not stressed during suturing and did not split; moreover, patch implantation into the defective wound was easy. No complications such as anastomotic leaks or infections occurred during implantation. One year post-implantation, the thickness of the Biosheet implantation section increased to approximately 2.5 mm, corresponding to approximately 70% of the native abdominal wall. A section of the abdominal wall muscle elongated from the periphery of the newly formed collagen layer, and the peritoneum was entirely formed on the peritoneal cavity surface, resulting in partial regeneration of the three-layered abdominal wall. The mechanical strength of the newly formed wall was approximately 5-fold higher than the native wall. The elasticity of the Biosheet in the low strain region decreased to approximately 10% post-implantation, similar to the native wall.

Biosheet maintained the abdominal wall without any complications for one year post-implantation, and partial regeneration was observed. Although this experiment was limited to two cases, the results indicated that Biosheet may serve as a reliable abdominal wall restorative material.

Chapter 4.

The iBTA tissues were able to control their thickness and mechanical properties at their in-body formation process and were shown to be adapted in-situ to the mechanical properties corresponding to the implantation sites.

List of Publications

The contents of this thesis are composed of the following papers.

Chapter 2-1.

Comparison of ethanol concentration as stock solution on mechanical properties of iBTA-induced collagenous tubular tissue "Biotube".

Terazawa T, Lai Yi-Ping, Tatsumi E, Nakayama Y.

J Biorheol. 2018; 32: 65-70

Chapter 2-2.

Wall thickness control in biotubes prepared using type-C mold.

Terazawa T, Nishimura T, Mitani T, Ichii O, Ikeda T, Kosenda K, Tatsumi E, Nakayama Y.

J Artif Organs. 2018; 21: 387-391

Chapter 2-3.

ヒト心膜の光干渉断層計による厚み分布計測と強度評価.

寺澤武・尾崎重之・中山泰秀

医工学治療. 2019; 31 (Accepted)

Characterization of an in-body tissue-engineered autologous collagenous sheet, Biosheet, for application as an aortic valve reconstruction material,

Terazawa T, Kawashima T, Umeno T, Wada T, Tatsumi E, Ozaki S, Miyamoto S, Nakayama Y.

(Manuscript in preparation)

Chapter 3-1.

Short-term evaluation of mechanical properties of the collagenous sheet (biosheet) after transplantation into beagle diaphragm

Terazawa T, MS, Nagatani K, DVM, Iimori Y, DVM, Akiyoshi H, DVM, PhD, Nakayama Y, PhD

(Manuscript in preparation)

Chapter 3-2.

One-Year Follow-Up Study of iBTA-Induced Allogenic Biosheet for Repair of Abdominal Wall Defects in a Beagle Model: a Pilot Study.

Terazawa T, Furukoshi M, Nakayama Y.

Hernia. 2018 (Epub ahead of print)

Other Related Papers (Not included in this thesis)

(1) Terazawa T, Nishimura T, Mitani T, Ichii O, Ikeda T, Kosenda K, Nakayama Y. Mechanical evaluation of the influence of subcutaneous implantation period of the mold on tissue maturation. (Manuscript in preparation)

(2) Umeda S, Nakayama Y, Terazawa T, Iwai R, Hiwatashi S, Nakahata K, Takama Y, Tatsumi E, Okuyama H. Long-term outcome of patch tracheoplasty using collagenous tissue membranes (Biosheets) produced by in-body tissue architecture (IBTA) in a beagle model. Surg Today. 2018 (Under article submission)

(3) Nakayama Y, Kaneko Y, Okumura N, Terazawa T, Tatsumi E. Initial 2-year results of first human use of an iBTA-induced autologous "Biotube" vascular graft in internal shunt restoration for haemodialysis. (Manuscript in preparation)

(4) 河島毅之，梅野惟史，岡本啓太郎，和田朋之，首藤敬史，寺澤武，中山泰秀，穴井博文，巽英介，宮本伸二．生体内組織形成術（IBTA）による大動脈弁再建術の開発．日本心臓血管外科学会雑誌 2018; 47: xxix-xxxiii

(5) Tracheal Replacement Using an In-Body Tissue-Engineered Collagenous Tube "BIOTUBE" with a Biodegradable Stent in a Beagle Model: A Novel Tracheal Scaffold.

Hiwatashi S, Nakayama Y, Umeda S, Takama Y, Terazawa T, Okuyama H.

Eur J Pediastr Surg. 2019; 29: 90-96

(6) Developing of Long in vivo tissue- engineered “Biotube” vascular grafts.

Nakayama Y, Furukoshi M, Terazawa T, Iwai R.

Biomaterials 2018; 185: 232-239.

(7) Patch esophagoplasty using an in-body-tissue-engineered collagenous connective tissue membrane.

Okuyama H, Umeda S, Takama Y, Terasawa T, Nakayama Y.

J Pediatr Surg. 2018; 53: 223-226

Acknowledgements

I would like to express the deepest appreciation to Professor Yasuhide Nakayama for his guidance, discussion, and constant support in helping me to conduct and complete this work. I would like to express my gratitude to Professor Hiroshi Hosoda for advice on research and daily support. I would like to thank Professor Mutsumi Takagi, Yota Murakami, and Kenichiro Matsumoto for serving on my advisory committee, as well as for their generous advice. I am grateful to Dr. Eisuke Tatsumi (Department of Artificial Organ, National Cardiovascular Center Research Institute) and Dr. Mariko Shiba (Department of Regenerative Medicine and Tissue Engineering) for prepared me the environment to study at the National Cardiovascular Research Center. I am indebted to Professor Takanori Nishimura (Research Faculty of Agriculture, Hokkaido University), Professor Shinji Miyamoto (Graduate School of Medicine, Oita University) and Professor Hideo Akiyoshi (Graduate School of Life and Environmental Sciences, Osaka Prefecture University) for their advice through collaborative research. In addition, I would like to thank Dr. Tsutomu Tajikawa (Department of Mechanical Engineering, Kansai University) and Dr. Tomonori Oie (Biotube Co., Ltd.) for advice on research. I thank Dr. Ryosuke Iwai (Okayama University of Science) for teaching the research techniques such as cell culture, Dr. Takeshi Moriwaki (Hirosaki University) for teaching how to use the 3D-CAD and many other instruments, and Ms. Maya Furukoshi for cooperation for experiments. I am grateful to the students of the Tajikawa Laboratory at Kansai University for active discussion at the time of the research meeting. Finally, my heartfelt appreciation goes to my wife, Kaori Terazawa and my children who have supported and encouraged me at any time.